Article

Cell Reports

HIV-1 Envelope Recognition by Polyreactive and Cross-Reactive Intestinal B Cells

Graphical Abstract

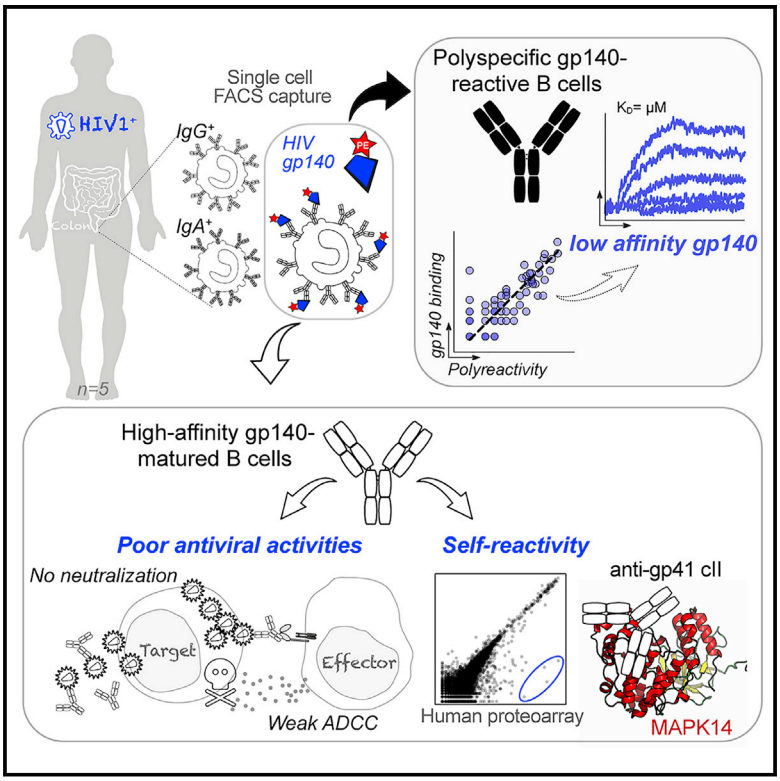

Highlights

- Polyreactive B cells in HIV-1^{+} intestinal mucosa interact with HIV-1 Env proteins
- High-affinity intestinal HIV-1 gp140 antibodies display poor antiviral activities
- Antibodies targeting the gp41 cluster II region cross-react with MAPK14

Authors

Cyril Planchais, Ayrin Kök, Alexia Kanyavuz, ..., Jordan D. Dimitrov, Laurent Hocqueloux, Hugo Mouquet

Correspondence

hugo.mouquet@pasteur.fr

In Brief

Antibodies produced in mucosa after sexual transmission of HIV-1 could affect viral propagation. Planchais et al. show that intestinal B cells from HIV-1-infected individuals that recognize the HIV-1 envelope (Env) proteins are mainly low affinity and polyreactive and that rare, high-affinity antibodies to HIV-1 Env lack potent antiviral capacities and cross-react with self-antigens.

Planchais et al., 2019, Cell Reports *27*, 572–585
April 9, 2019
https://doi.org/10.1016/j.celrep.2019.03.032

CellPress

OPEN ACCESS
CellPress

Cell Reports
Article

HIV-1 Envelope Recognition by Polyreactive and Cross-Reactive Intestinal B Cells

Cyril Planchais,[1,2,11] Ayrin Kök,[1,2,11] Alexia Kanyavuz,[3,4,5] Valérie Lorin,[1,2] Timothée Bruel,[6,7] Florence Guivel-Benhassine,[6,7] Tim Rollenske,[8] Julie Prigent,[1,2] Thierry Hieu,[1,2] Thierry Prazuck,[9] Laurent Lefrou,[10] Hedda Wardemann,[8] Olivier Schwartz,[6,7] Jordan D. Dimitrov,[3,4,5,12] Laurent Hocqueloux,[9,12] and Hugo Mouquet[1,2,13,*]

[1]Laboratory of Humoral Immunology, Department of Immunology, Institut Pasteur, Paris 75015, France
[2]INSERM U1222, Paris 75015, France
[3]Sorbonne Universités, UPMC Université Paris 06, UMR_S 1138, Centre de Recherche des Cordeliers, Paris 75006, France
[4]INSERM, UMR_S 1138, Centre de Recherche des Cordeliers, Paris 75006, France
[5]Université Paris Descartes, Sorbonne Paris Cité, UMR_S 1138, Centre de Recherche des Cordeliers, Paris 75006, France
[6]Virus & Immunity Unit, Department of Virology, Institut Pasteur, Paris 75015, France
[7]CNRS URA3015, Paris, 75015, France
[8]Division of B Cell Immunology, German Cancer Research Center, Heidelberg 69120, Germany
[9]Service des Maladies Infectieuses et Tropicales, CHR d'Orléans-La Source, Orléans 45067, France
[10]Service d'Hépato-Gastro-Entérologie, CHR d'Orléans-La Source, Orléans 45067, France
[11]These authors contributed equally
[12]These authors contributed equally
[13]Lead Contact
*Correspondence: hugo.mouquet@pasteur.fr
https://doi.org/10.1016/j.celrep.2019.03.032

SUMMARY

Mucosal immune responses to HIV-1 involve the recognition of the viral envelope glycoprotein (gp) 160 by tissue-resident B cells and subsequent secretion of antibodies. To characterize the B cells "sensing" HIV-1 in the gut of infected individuals, we probed monoclonal antibodies produced from single intestinal B cells binding to recombinant gp140 trimers. A large fraction of mucosal B cell antibodies were polyreactive and showed only low affinity to HIV-1 envelope glycoproteins, particularly the gp41 moiety. A few high-affinity gp140 antibodies were isolated but lacked neutralizing, potent ADCC, and transcytosis-blocking capacities. Instead, they displayed cross-reactivity with defined self-antigens. Specifically, intestinal HIV-1 gp41 antibodies targeting the heptad repeat 2 region (HR2) cluster II cross-reacted with the p38α mitogen-activated protein kinase 14 (MAPK14). Hence, physiologic polyreactivity of intestinal B cells and molecular mimicry-based self-reactivity of HIV-1 antibodies are two independent phenomena, possibly diverting and/or impairing mucosal humoral immunity to HIV-1.

INTRODUCTION

Mucosal antibodies are essential in maintaining host-microbial homeostasis and protecting from invading pathogens (Kubinak and Round, 2016; Lycke and Bemark, 2017; Spencer and Sollid, 2016). Early during HIV-1 infection, massive depletion of gut $CD4^+$ T cells, notably follicular T helper cells (TFH), and loss of germinal centers in mucosa-associated lymphoid tissues impair the induction of antibody responses (Chaoul et al., 2012; Levesque et al., 2009; Mehandru et al., 2004). Bacterial translocation and subsequent immune activation and/or inflammation in the mucosa of infected individuals may also weaken local humoral immunity (Dillon et al., 2016; Klatt et al., 2013; Ponte et al., 2016). Nonetheless, early antiretroviral therapy (eART) partially prevents HIV-1-induced mucosal damages and immune dysregulation (Costiniuk and Angel, 2012; Kök et al., 2015; Ponte et al., 2016). eART allows preserving functional gut TFH and resting memory B cells specific to glycoprotein (gp)140 trimers (Planchais et al., 2018). Mucosal transmission of HIV-1 induces a local production of immunoglobulin (Ig)G and IgA antibodies that predominantly target the gp41 subunit of the viral envelope glycoprotein gp160 (Trama et al., 2014; Yates et al., 2013). However, whether they limit viral dissemination upon HIV-1 exposure is unclear (Astronomo et al., 2016; Cheeseman et al., 2016; Tudor et al., 2009). Polyreactive antibodies naturally produced by intestinal B cells and coating commensals *in situ* have been proposed to compromise optimal humoral responses to HIV-1 by immune diversion (Bunker et al., 2017). However, overall, very little is known about the antibody response to HIV-1 at mucosal sites and the properties of gut-resident B cells recognizing the virus.

Single-cell, antigen-specific capture and expression cloning of human antibodies greatly facilitated decoding systemic memory B cell responses to gp140 in HIV-1-infected individuals (Mouquet, 2014). This also allowed the discovery of broadly neutralizing antibodies with *in vivo* prophylactic and therapeutic efficacy (Cohen and Caskey, 2018). However, the humoral response to HIV-1 in mucosal tissues was never, to our knowledge, investigated with antigen-baiting strategies for characterizing

gp140-reactive B cell antibodies. Here, we interrogated the intestinal B cell response to HIV-1 by characterizing 76 recombinant monoclonal antibodies from gp140-binding IgA^+ and IgG^+ B cells from rectosigmoid colon tissues of HIV-1-infected individuals. We show that most mucosal B cell antibodies are polyreactive, displaying only a low affinity to gp160. High-affinity, intestinal HIV-1 antibodies were also identified but lacked antibody-dependent cellular cytotoxicity (ADCC) potency against transmitted founder (T/F) viruses, did not neutralize HIV-1 or block its transcytosis across mucosal epithelium, and cross-reacted with self-antigens. This suggests an inability of the gut immune system to locally generate functional high-affinity antibodies in response to HIV-1 infection.

RESULTS

Capture of HIV-1-Reactive Intestinal B Cells from Infected Individuals

To characterize HIV-1-reactive B cells residing in tertiary lymphoid structures of the intestinal mucosa, we obtained colorectal biopsies from five $HIV\text{-}1^+$ individuals, four of them being infected with clade-B viruses (Table S1). All donors had serum IgG antibodies to trimeric gp140, gp120, and gp41 proteins with no detectable *in vitro*, neutralizing activity (Figures 1A and 1B). As expected, blood class-switched (CS) B cells were mostly IgG^+ (16.6% versus 5.3% for IgA^+), whereas CS memory B cells and plasmablasts in the intraepithelial lymphocyte (IEL) and lamina propria lymphocyte (LPL) compartments expressed predominantly surface IgAs (14.6% and 17% versus 9.3% and 13.4% for IgG^+ cells, respectively) (Figures 1C, S1A, and S1C). Flow-cytometric immunophenotyping showed equal proportions of mature naive (MN) and resting memory (RM) B cells in the IEL compartment (36.5% versus 41.3%) but about twice more RM than MN B cells in the LPL (48.6% versus 25.4%) (Figures 1D and S1B). Mucosal IgA^+ and IgG^+ B cells were stained with fluorescently labeled, clade-B, YU-2 gp140 trimers (Figures 1E, S1D, and S1E). The vast majority of gp140-reactive mucosal B cells expressed surface IgA and mainly originated from the *lamina propria* for the non-treated (NT) and late-treated ART (lART) patients and from the IEL compartment for the early treated (eART) patient (Figure 1F). Immunoglobulin gene analyses showed that apart from an enrichment of V_H1 gene usage in gp140-captured mucosal B cells, which mostly originated from lART-derived cells (27%; particularly V_H1–18 and V_H1–46 genes), no major variations were observed when compared with healthy blood and mucosal, global, B cell repertoires (Benckert et al., 2011; Prigent et al., 2016) (Figure S2; Table S2). These B cells displayed relatively high levels of somatic mutations in IgH and IgL variable gene segments, with more mutated antibodies isolated from lART donors (Figure S2F; Table S2).

Mucosal Non-neutralizing HIV-1 Antibodies Lack Potent ADCC Activity against T/F Viruses

Only 4 of the 76 antibodies produced bound to YU-2 gp140 trimers with high affinity (Figure 1G; Table S2). Three of them were specific for the gp41 subunit (Figure 2A); 6-159 bound to the putative immunodominant peptide (PID), whereas 6-195 and 64-i109 reacted against conformational gp41 epitopes (Figure 2B). ELISA binding analyses on gp120 mutant proteins indicated that 6-104 targets the CD4-induced site (CD4i) (Figure 2B). None of the mucosal HIV-1 antibodies, either expressed as IgG or IgA (as found *in situ* for 6-159 and 6-195), had measurable *in vitro* neutralizing activity against a five-virus panel (Figure 2C). Non-neutralizing HIV-1 antibodies (nnAbs) can exert ADCC activity against HIV-1-infected target cells (Bruel et al., 2017; Horwitz et al., 2017; Richard et al., 2018). Because the killing process requires opsonization of target cells, we first examined the binding of mucosal HIV-1 antibodies to $CD4^+$ T cells infected with three laboratory-adapted and six T/F viruses. In agreement with our previous work (Bruel et al., 2017), nnAbs bound well to cells infected with laboratory-adapted strains but only poorly to T/F-infected cells (Figures 2D and S3). As previously reported for prototypical anti-PID 5-25 (Bruel et al., 2017), the strongest binding was observed with 6-159, which stained most cells infected with laboratory-adapted viral strains (81%–86%), but only 0.5%–17% of those harboring T/F virions (Figures 2D and S3). Consistent with binding data, 6-159 and, to a lesser extent, the other mucosal HIV-1 nnAbs induced ADCC-mediated killing of targets cells infected by laboratory-adapted strain NL4.3 (64% and 29%–35%, respectively) (Figure 2E). However, mucosal IgGs displayed weak ADCC activities against CH058 and CH077 T/F viruses compared with 3BNC117 and PGT128 broadly neutralizing antibodies (bNAbs) (Figure 2E). Mucosal nnAbs did not block HIV-1 transcytosis across epithelial cell monolayers (Figure 2F) and, in contrast to bNAbs (Lorin et al., 2017), they did not neutralize transcytosed virions (Figure 2G). All gp41 nnAbs showed interactions with colon-prominent mucin 2, but only 6-159 was able to capture free T/F virions (Figures 2H and 2I), suggesting that mucosal anti-PID antibodies could have the ability to trap incoming HIV-1 viruses into mucosa-associated mucin networks.

Polyreactive Blood and Mucosal B Cell Antibodies from Non-Infected Humans Recognize HIV-1 Envelope Glycoproteins

Only a small fraction of the captured B cell antibodies recognized gp140 trimers with high affinity. We thus wondered whether the 72 remaining ones were enriched for polyreactive clones with low affinity for HIV-1 envelope (Env) glycoproteins. Polyreactivity analyses showed that 33% of the mucosal antibodies showed similar levels of ELISA reactivity with structurally unrelated non-HIV-1 molecules (Figure 3A). Polyreactive antibodies also bound to HIV-1 trimeric gp140, gp120, and gp41 proteins (Figures 3B and S4A). None of the mucosal antibodies showed reactivity against human epithelial type 2 (HEp-2) cells by the indirect immunofluorescence assay routinely used in clinical diagnostics for autoantibody detection (Table S2). We next tested whether non-HIV antibodies from blood IgA^+ and IgG^+ memory B cells of healthy individuals (n = 124) (Prigent et al., 2016) recognized HIV-1 Env proteins. IgG antibodies weakly bound to HIV-1 gp140 trimers, gp120, and gp41 subunits with a reactivity pattern consistent with polyreactivity (Figures 3C and 3D). Of note, the binding intensity to HIV-1 Env proteins, more particularly gp41, was consistently greater than the one measured for non-HIV-1 ligands (Figures 3B and 3D). Most polyreactive intestinal antibodies from IgA^+ and IgG^+ plasmablasts of uninfected

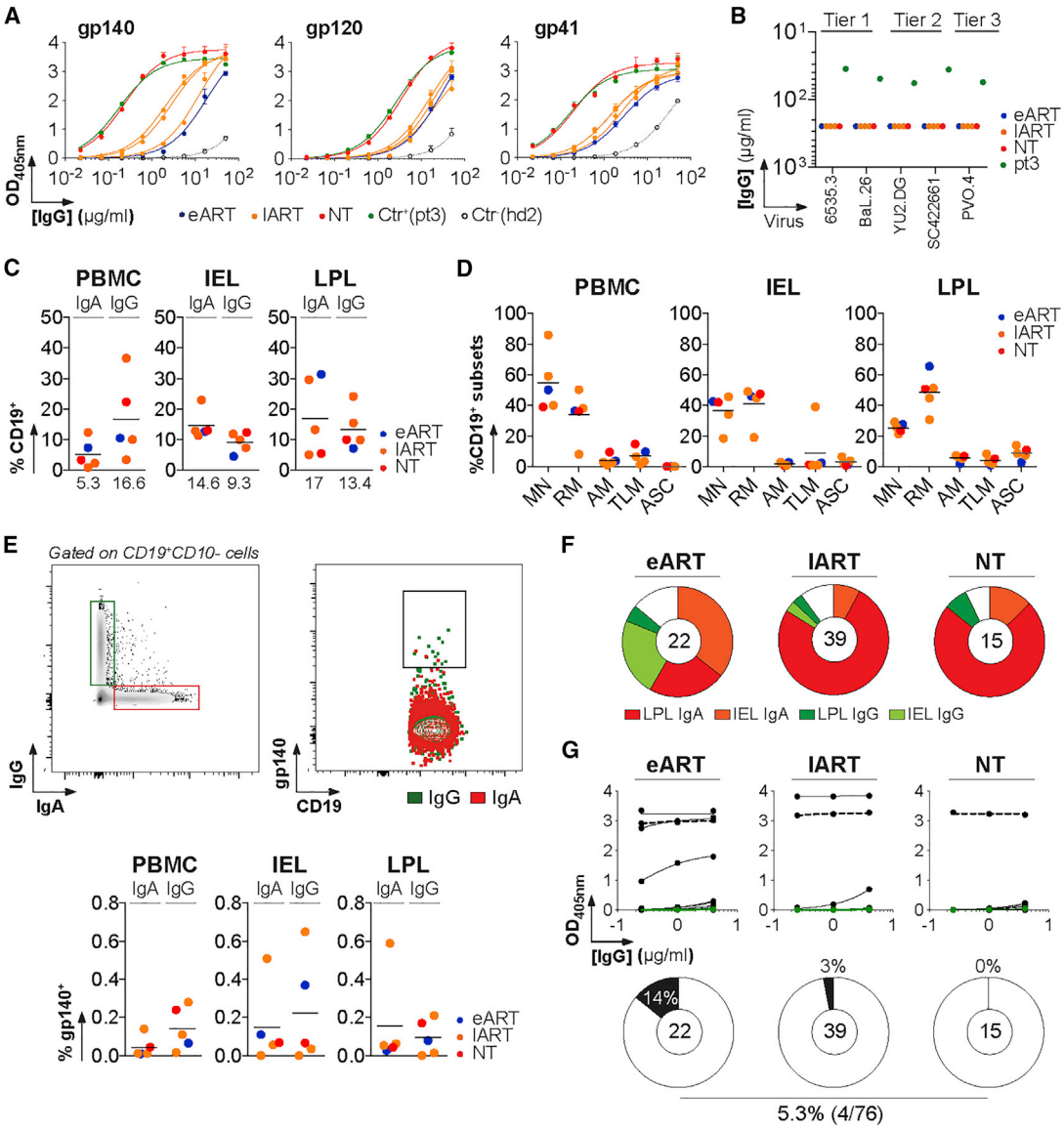

Figure 1. Capture of HIV-1 Env-Reactive Mucosal B Cells

(A) Representative ELISA graph showing the reactivity of purified serum IgG (sIgG) from HIV-1-infected individuals (n = 5) against trimeric gp140, gp120, and gp41 proteins. Error bars indicate the SEM of duplicate values. Ctr^+, positive control sIgG; pt3, patient 3 (Scheid et al., 2009); Ctr^-, negative control sIgG; hd2, healthy donor 2 (Prigent et al., 2016).

(B) Neutralization activity of sIgG from HIV-1-infected donors (n = 5) measured by TZM-bl assay.

(C) Dot plots comparing the percentage of IgA^+CD19^+ and IgG^+CD19^+ cells in the IEL, LPL, and peripheral blood mononuclear cell (PBMC) compartments determined by flow cytometry as shown in Figure S1. Median values are indicated below.

(D) Dot plots comparing the distribution of B cell subsets in the IEL, LPL, and PBMC compartments determined by flow cytometry as shown in Figure S1. Percentage of mature naive (MN), resting memory (RM), activated memory (AM), and tissue-like memory (TLM) B cells and antibody-secreting cells (ASC) are shown.

(E) HIV-1 gp140-reactive B cell fluorescence-activated cell sorting (FACS). (Top) Cytograms show the gating strategy used for single-cell sorts of gp140-binding mucosal B cells. An example is given for patient COA21. (Bottom) Dot plots comparing the percentage of gp140-reactive IgA^+ and IgG^+ $CD19^+$ lymphocytes from the IEL, LPL, and PBMC compartments determined by flow cytometry as shown in Figure S1.

(F) Pie charts show the distribution of single gp140-binding B cells captured by FACS with YU-2 gp140 trimers among IEL and LPL IgA^+ and IgG^+ B cell populations. The number of B cells captured is indicated in the center of each pie chart.

(G) Representative ELISA graph showing the reactivity of gp140-captured mucosal monoclonal antibodies (mAbs; n = 76) against YU-2 gp140 trimers. Error bars indicate the SEM of duplicate values. Dotted black and green lines represent the positive control 10-1074 and negative control mGO53 IgG antibodies, respectively. The proportion of high affinity anti-gp140 antibodies in each patients' group is shown below in the pie charts. The total number of tested antibodies is indicated in the center of each pie chart.

See also Figures S1 and S2 and Tables S1 and S2.

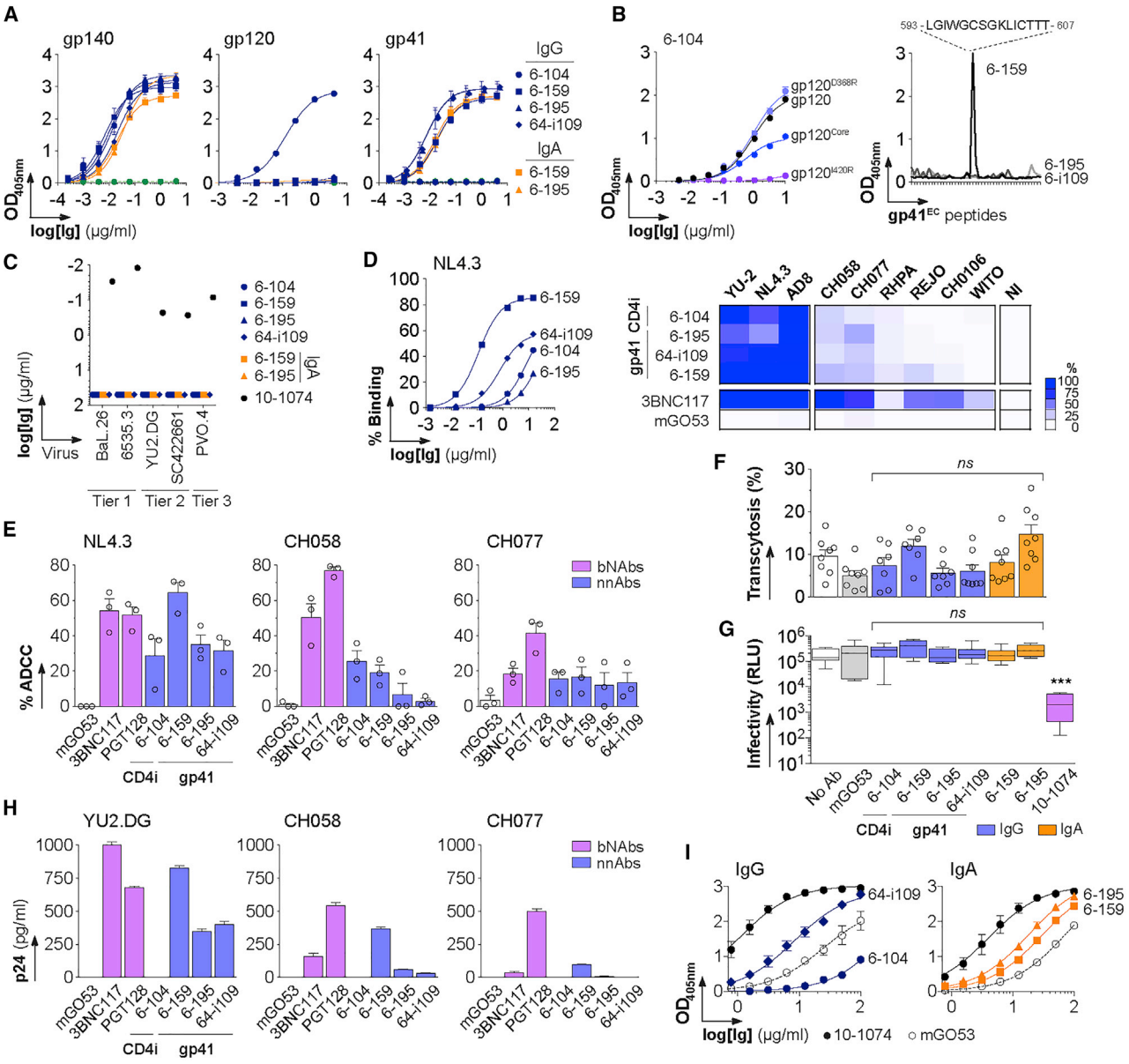

Figure 2. Epitopes and Antiviral Activities of Mucosal HIV-1 gp140 Antibodies

(A) Representative ELISA graphs show the binding of mucosal HIV-1-specific antibodies to trimeric gp140, gp120 and gp41 proteins. Error bars indicate the SEM of quadruplicate values. The green dotted line corresponds to the negative control antibody mGO53.

(B) Epitope mapping. (Left) Representative ELISA graph comparing the binding of anti-gp120 antibody 6-104 to wild-type gp120, gp120^{core}, gp120^{D368R}, and gp^{I420R} mutant proteins. Error bars indicate the SEM of quadruplicate values. (Right) Representative ELISA graph shows the reactivity of mucosal anti-gp41 monoclonal antibodies (mAbs) against overlapping peptides covering the extracellular portion of gp41 (gp41^{EC}). The sequence of the peptide recognized by 6-159 is indicated on the top.

(C) Plot shows the neutralization activity of mucosal gp140-specific mAbs as measured in duplicate in two independent *in vitro* TZM-bl assay experiments (one representative is shown).

(D) Antibody binding to infected target cells. (Left) Graph shows the binding of anti-gp140 IgGs to NL4.3-infected cells, measured as the percentage of IgG$^+$ in Gag$^+$ cells by flow cytometry. (Right) Heat map comparing the percentage of bound, infected cells (n = 9 viruses) by antibodies (at 15 μg/ml) assayed by flow cytometry as shown in Figure S3. 3BNC117 and mGO53 are positive and negative control, respectively.

(E) Bar graphs comparing the ADCC activity of HIV-1 nnAbs and bNAbs (PGT128 and 3BNC117) against target cells infected by selected viruses as measured by flow cytometry. Mean values (dots) ± SEM of three independent experiments performed in duplicate are shown. mGO53 is the non-HIV-1 isotype control.

(F) Bar graph shows the percentage of transcytosis of NLAD8 alone (white, no antibody), in the presence of non-HIV-1 mGO53 control (gray), HIV-1 bNAb 10-1074, and mucosal HIV-1 antibodies expressed as monomeric IgG (blue) and IgA (orange) antibodies. Mean values ± SEM of quadruplicate values from two independent experiments (dots) are shown.

(legend continued on next page)

individuals (n = 41) (Benckert et al., 2011) also reacted against HIV-1 Env glycoproteins (90% against gp140 and gp41) (Figure 3E). We next determined the relative affinity of polyreactive non-HIV-1 antibodies (18-295, HD1a361, and HD2a57 (Benckert et al., 2011), plus historical polyreactive control ED38 (Meffre et al., 2004)) to YU-2 and ZM96 trimers by surface plasmon resonance (SPR) (Figures 3F and S4C). K_D values could only be derived for the binding to YU-2 gp140 and ranged from 30.5 to 53.9 nM (versus 0.03–0.2 nM for gp140-specific antibodies; Figures 3F and S4C). Compared with high-affinity gp140 antibodies, polyreactive gp140-reactive IgGs displayed about a log decrease of the association rate and a 300-fold faster dissociation to the HIV-1 Env (Figure 3F). Flow cytometry analyses confirmed the weak, but detectable, binding of polyreactive antibodies to Env proteins exposed at the surface of HIV-1-infected cells (Figures 3G and S4D).

Mucosal HIV-1 Env Antibodies Cross-React with Human Autoantigens

Circulating blood and mucosal HIV-1-specific B cell antibodies are often polyreactive and cross-reactive with self-antigens (Mouquet and Nussenzweig, 2012; Trama et al., 2014). The intestinal anti-gp41 IgGs cloned here displayed very weak (6-159 and 64-i109) to marked (6-195) polyreactivity (Figures 4A and S5A). None of the mucosal anti-gp140 showed detectable reactivity against HEp-2-expressing antigens by IFA (Figure 4B), or immunoblotting (not shown). We next probed the reactivity of the antibodies with microarrays containing more than 9,000 human proteins (Figures 4C, 4D, and S5B). Binding analyses confirmed the slight polyreactivity of 6-195, characterized by a global shift of the fluorescence signals compared with the isotype control mGO53 (Figure 4C). Interestingly, three HIV-1 antibodies had strong cross-reactivity to a limited set of human proteins in two independent experiments (Figures 4D and S5B). The immunoreactive proteins with the greatest binding (Z scores > 5) were tyrosine-protein phosphatase non-receptor type 2 (PTPN2) and SMAD family members 2 and 3 (SMAD2 and SMAD3) for 6-104; mitogen-activated protein kinase 14 (MAPK14) for 6-195; nudE nuclear distribution gene E homolog like 1 (NDE1); and RUN and FYVE domain-containing 3 (RUFY3) for 64-i109 (Figures 4D and S5B). Of note, MAPK14 was also recognized weakly by anti-gp41 antibody 64-i109 (Z = 1.2) (Figure S5B). ELISA analyses confirmed MAPK14 cross-reactivity of 6-195 and, to a lesser extent, of 64-i109, whereas no binding was detected for 6-104 and 6-159 (Figure 4E). Indeed, 6-195 showed high-affinity binding to MAPK14 by SPR with a K_D of 26.5 nM (Figure 4F), whereas no significant interactions were observed with 64-i109 (not shown).

Mucosal and Blood HIV-1 Antibodies Cross-Reacting with MAPK14 Target the gp41 Heptad Repeat 2 Region

Clonal variants of HIV-1 B cell lineages can be shared between blood and mucosa compartments (Sacha et al., 2015; Trama et al., 2014). Circulating and intestinal B cell clones can also target independently the same epitope on HIV-1 Env. We, therefore, wondered whether blood-derived gp41-specific antibodies display cross-reactivity to human antigens, particularly against MAPK14. Nine blood anti-gp41 antibodies isolated from IgG^+ memory B cells of HIV-1-infected individuals (Mouquet et al., 2011; Scheid et al., 2009) were randomly selected for binding to protein microarrays. Most of them recognized conformational epitopes (6-161, 10-137, 10-325, 10-647, 10-679, and 10-1304), whereas 5-25 and 10-1487 bound to the PID peptide (Mouquet et al., 2011; Scheid et al., 2009), and 10-437 bound to a linear epitope in the gp41 polar region (Figure 5A); 6-161 was previously mapped to the C-terminal heptad repeat or heptad repeat 2 (HR2) region of gp41 ($gp41^{HR2}$) (Pietzsch et al., 2010; Scheid et al., 2009). Cross-competition ELISA experiments confirmed that the epitopes of mucosal 6-195 and 64-i104 and blood 10-325, 10-647, and 10-679 are also located in gp41 HR2 (Figure 5B). Four of the blood gp41 IgGs showed polyreactivity on protein microarrays, from low to medium (10-679 and 6-161) to very high pan-reactivity as polyreactive control ED38 (10-325 and 10-1487) (Figures 5C and S6A). Blood gp41 antibodies did not cross-react with specific human proteins (Figures 5C and S6B); 6-161, 10-325, and 10-1487 displayed binding to MAPK14 (Figure 5C) but were normalized to baseline because of their global pan-reactivity on microarrays (Figure 5D). Nonetheless, ELISA and SPR analyses confirmed that only anti-$gp41^{HR2}$ antibodies, and no other anti-gp41 IgGs, except highly polyreactive 10-1487 (n = 6), bound with varying affinities to purified recombinant MAPK14 (Figures 5E and 5F). The apparent affinity (K_D) of gp41 antibodies 10-679, 6-161, 10-647, 6-195, 10-325, and 10-1487 to MAPK14 ranged from 130 to 10.5 nM (Figure 5F). MAPK14-reactive anti-$gp41^{HR2}$ antibodies were distinct from previously described polyreactive mucosal antibodies specific to the gp41 cluster I that cross-react with *Escherichia coli* RNA polymerase (Liao et al., 2011; Trama et al., 2014) (Figures S5C–S5E).

HIV-1 gp41 HR2 Cluster II Antibodies Bind to MAPK14 via Electrostatic Interactions

The gp41 HR2 contains two epitopic clusters, cluster II and VI, the former being frequently targeted by monoclonal antibodies from Env-immunized mice (Earl et al., 1997) and HIV-1 infected humans (Pietzsch et al., 2010). Competition ELISA experiments with mouse anti-cluster II antibody D50 (Earl et al., 1997) confirmed that the epitopes of the anti-$gp41^{HR2}$ IgGs

(G) Scatter plot shows the infectivity level of transcytosed NLAD8 viruses derived from the experiments shown in (F) on TZM-bl reporter cells. Antibodies were tested at a final concentration of 66.7 nM. RLU, relative light units. Groups in (F) and (G) were compared to the no-antibody control by the Mann-Whitney test. ns, not significant; ***$p < 0.001$.

(H) Bar graphs show the amount of free viruses captured by mucosal HIV-1 and control antibodies measured by ELISA as p24 content. Mean of quadruplicate values ± SEM are shown.

(I) ELISA graphs show the binding of mucosal HIV-1 and control antibodies to purified human mucin 2. Mean values ± SEM of two independent experiments performed in duplicate are shown.

See also Figure S3.

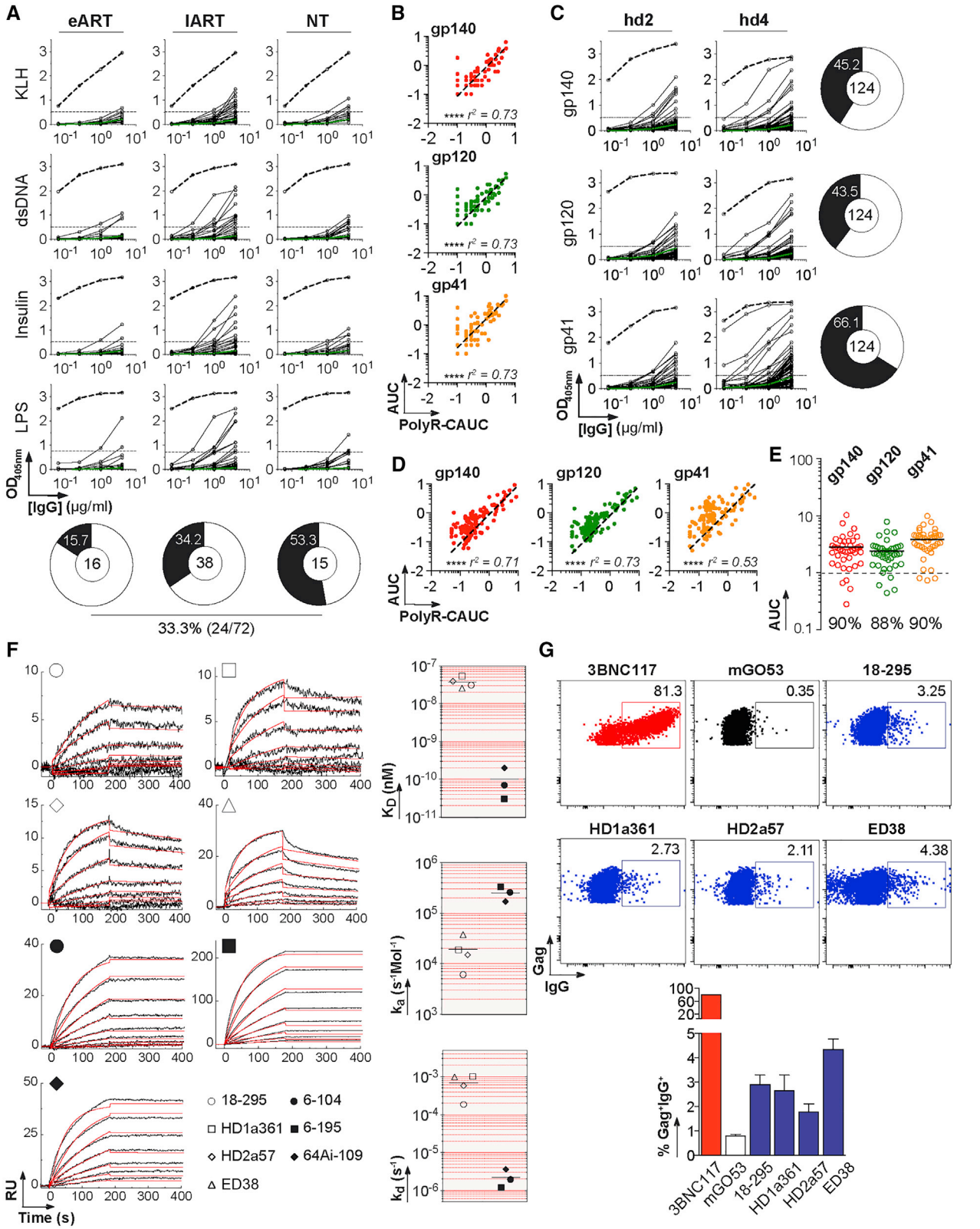

(legend on next page)

cross-reacting with MAPK14 are located in cluster II (Figure 6A). Accordingly, D50, as well as previously described human anti-cluster II antibodies 167-D IV (Xu et al., 1991), 98-6 (Gorny et al., 1989), and 5F3 (Buchacher et al., 1994), showed ELISA binding to purified MAPK14 (Figure 6B). This portion of the HR2 (amino acids 642–665) is enriched in charged and polar residues acids, especially glutamic and aspartic acids (Figures 6C and 6E), suggesting that cluster II-specific antibodies bind to gp41 via electrostatic interactions. In contrast to polyreactive ED38 and 10-1487 antibodies, anti-gp41^{HR2} IgGs were sensitive to changes in the ionic environment, as evidenced by the decreased ELISA reactivity to MAPK14 with increased salt concentrations (Figure 6D), indicating that they cross-reacted with MAPK14 through the formation of electrostatic bonds. ELISA binding analyses on Env proteins from different HIV-1 strains showed that E662A substitution affects the reactivity of D50 and 98-6 IgGs but not that of the other anti-gp41^{HR2} cluster II antibodies (Figure 6E). Although no common peptide sequences unambiguously matched gp41 and MAPK14, structural alignment analysis showed an α helices superimposition identifying a putative mimicry motif (D/ELLE) between gp41^{HR2} cluster II and MAPK14 (Figure 6F). This peptide candidate is interesting because it encompasses the gp160 residue E662, which is crucial for the binding of D50 and 98-6 antibodies to gp41, and because it contains two aspartic or glutamic acid residues that could promote electrostatic interactions with gp41^{HR2} cluster II IgGs. Nevertheless, because the ELLE motif is short, even if it really contributed to the cross-reactivity of some anti-gp41^{HR2} cluster II antibodies, additional interactions with unidentified homologous protein patches might be involved in the process. Finally, germline versions of 10-325, 6-195, and 64-109 antibodies failed to react with trimeric gp140 and gp41 proteins and simultaneously displayed reduced to abrogated MAPK14 binding, implying that somatic hypermutation is required for the recognition of both HIV-1 gp160 and MAPK14 (Figure 6G).

DISCUSSION

In this study, we captured Env-reactive B cells from colorectal tissues of HIV-1-infected patients. The isolated high-affinity gp140 antibodies targeted mainly gp41 and lacked neutralizing activity, potent ADCC breadth, and blocking capacity against HIV-1 transcytosis. In contrast to HIV-1 bNAbs (Lorin et al., 2017), mucosal HIV-1 nnAbs did not suppress post-transcytosis infectivity *in vitro*. Although HIV-1 nnAbs may modestly diminish the number of transmitted viruses (Santra et al., 2015), recent reports demonstrated that viral neutralization is required to confer protection against mucosal HIV-1 transmission *in vitro* and *in vivo* (Astronomo et al., 2016; Cheeseman et al., 2016). Moreover, in contrast to certain HIV-1 bNAbs, most nnAbs do not exhibit optimal Fc-dependent antiviral effector functions against T/F-infected cells (Bruel et al., 2016; Bruel et al., 2017) because they cannot interact with the fully closed state of the viral envelope. Nevertheless, anti-PID antibodies, such as 6-159, are able to bind to a substantial fraction of free and cell-associated T/F viruses, most likely via gp41 stumps recognition (Bruel et al., 2016; Bruel et al., 2017). In mucosal tissues, they could participate in eliminating both IgG-bound free virions captured in mucus and HIV-1-infected cells through ADCC and/or antibody-dependent cellular phagocytosis mechanisms. Despite a prototypical anti-PID antibody having been shown to promote *in vivo* clearance of infected cells in humanized mice (Bruel et al., 2017; Horwitz et al., 2017; Richard et al., 2018), it remains unclear whether mucosal nnAbs have antiviral activity *in situ* and whether they can alter the course of HIV-1 transmission in humans. On the other hand, mucosa-derived milk anti-gp120 IgG antibodies have antiviral properties and could decrease HIV-1 transmission from infected, lactating women to infants (Fouda et al., 2011; Mabuka et al., 2012). Recombinant mucosal gp120-specific IgGs produced from milk-resident B cells may be neutralizing or ADCC potent (Friedman et al., 2012; Jeffries et al., 2016; Sacha et al., 2015). Hence, although gut and

Figure 3. Polyreactivity and Binding to HIV-1 Env Glycoproteins

(A) ELISA graphs show the reactivity of mucosal antibodies isolated from HIV-1-infected individuals (n = 72) against keyhole limpet hemocyanin (KLH), double-stranded DNA (dsDNA), insulin, and lipopolysaccharide (LPS). mGO53 (green lines) and ED38 (dotted lines) are negative and positive control antibodies, respectively. Horizontal lines show cutoff optical density 405 ($OD_{405\ nm}$) for positive reactivity.

(B) Correlation plots comparing the polyreactivity and the reactivity to HIV-1 Env proteins of mucosal antibodies. The y axis indicates the area under the curve (AUC) values of the ELISA binding curves shown in Figure S4A. The x axis indicates cumulative area under the curve (CAUC) values for polyreactivity (polyR) as measured in (A) against all four antigens. Bivariate correlations were estimated with the two-tailed Pearson correlation test. ****$p < 0.0001$.

(C) ELISA graphs show the reactivity of IgA^+ and IgG^+ memory B cell antibodies from healthy individuals hd2 and hd4 (n = 124) (Prigent et al., 2016) against trimeric gp140, gp120, and gp41 proteins. mGO53 (green lines) and ED38 (dotted lines) are negative and positive control antibodies, respectively. Horizontal lines show cutoff $OD_{405\ nm}$ for positive reactivity. The proportion of antibodies reactive against each HIV-1 protein is shown in pie charts (right), with the total number of antibodies tested indicated in the center.

(D) Same as in (B) but for memory B cell antibodies from healthy individuals.

(E) Dot plot shows the reactivity of intestinal IgA^+ and IgG^+ plasmablast mAbs from healthy individuals (n = 41) (Benckert et al., 2011) against trimeric gp140, gp120 and gp41 proteins. The y axis indicates the AUC values of the ELISA binding curves shown in Figure S4B. The dotted line represents the positive threshold, and the percentages of binders are indicated below each group.

Mean values from two independent experiments are shown in (A)–(E).

(F) (Left) SPR sensorgrams comparing the binding of selected antibodies (n = 7) to trimeric YU-2 gp140 glycoproteins. The y axis shows the resonance units (RU) obtained at a given time (s, seconds) indicated on the x axis. (Right) Dot plots comparing the relative affinity (K_D) and kinetics constants (k_a, k_d) of selected antibodies to trimeric YU-2 gp140 glycoproteins.

(G) (Top) Cytograms show the binding of selected IgG antibodies to Gag^+ YU-2-infected cells. (Bottom). Graph comparing the percentage of antibody binding to YU-2 virions exposed at the surface of infected target cells as measured by flow cytometry. mGO53 is the non-HIV-1 isotype control. Error bars indicate the SEM of triplicate values.

See also Figure S4.

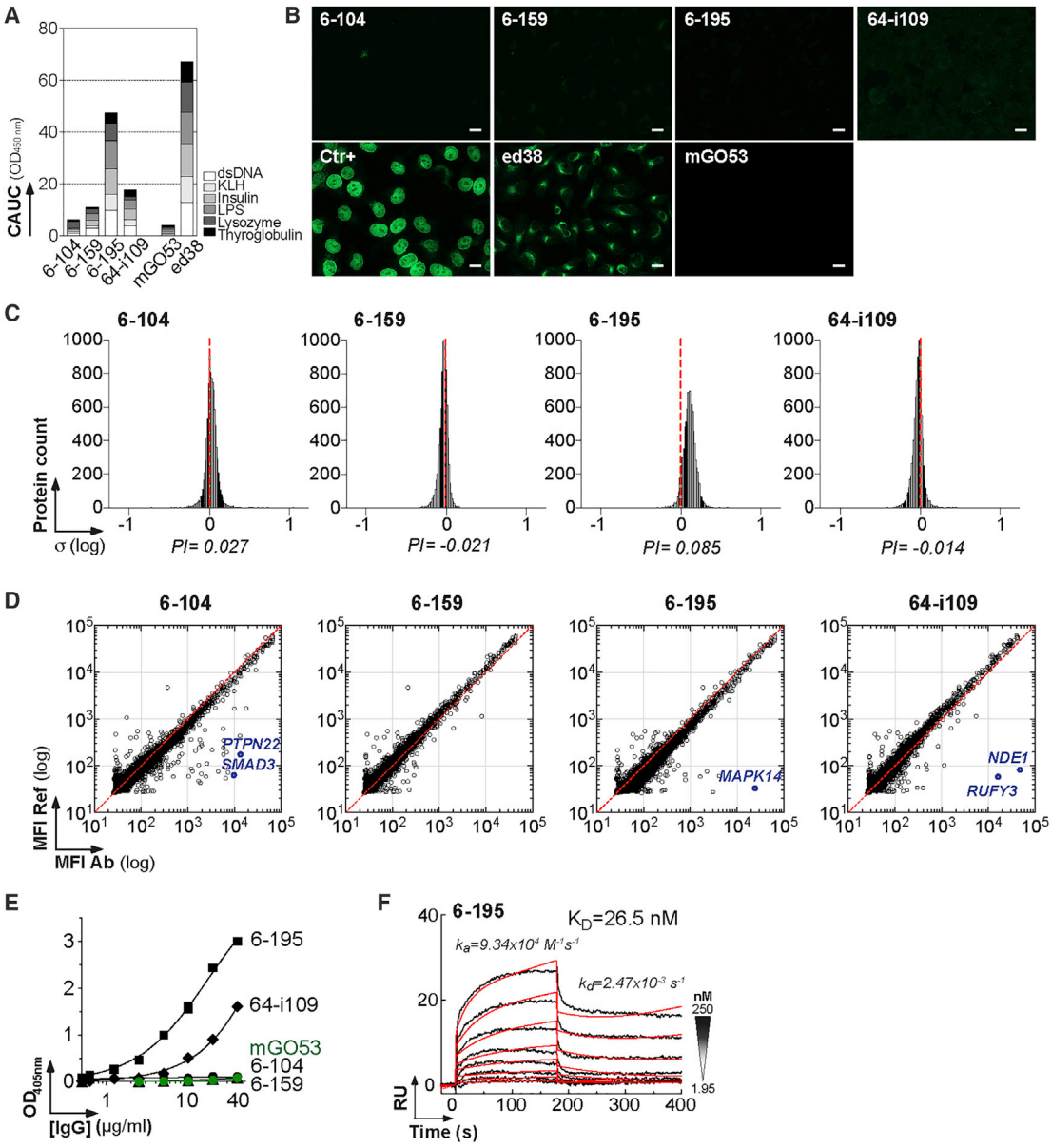

Figure 4. Cross-Reactivity of Mucosal HIV-1 Antibodies against Human Self-Antigens

(A) Bar graph shows the polyreactivity levels of mucosal HIV-1 gp140 antibodies as measured in duplicate by ELISA against KLH, dsDNA, insulin, and LPS in Figure S5A. The x axis indicates cumulative AUC (CAUC) values for polyreactivity (polyR).

(B) Antibody binding to HEp-2 cells was assayed by immunofluorescence assay. Ctr^{+}, positive control of the kit. mGO53 and ED38 are negative and positive control antibodies, respectively. The scale bars represent 15 μM.

(C) Frequency histograms show the $\log_{10}$ protein displacement (σ) of the mean fluorescent intensity (MFI) signals for the selected antibodies (n = 9) compared with non-reactive antibody mGO53. The polyreactivity index (PI) corresponds to the Gaussian mean of all array protein displacements.

(D) Representative protein microarray plots show the reactivity profile of mucosal anti-gp140 antibodies against human proteins. For each protein spot, the MFI given by the reference (mGO53) and test are depicted on the y and x axes, respectively. Each dot represents the average of duplicate array proteins. The diagonal lines indicate equal binding for reference and test antibodies. Blue dots indicate immunoreactive proteins with a *Z* score > 5 that were identified in two independent experiments as shown in Figure S5B.

(E) Representative ELISA graph comparing the reactivity of mucosal anti-gp140 antibodies to purified MAPK14. mGO53 is the negative control (green). Error bars indicate the SEM of duplicate values.

(F) SPR sensorgram showing the binding overtime of 6-195 to purified MAPK14 proteins immobilized on the sensor chip (50 RUs).

See also Figure S5.

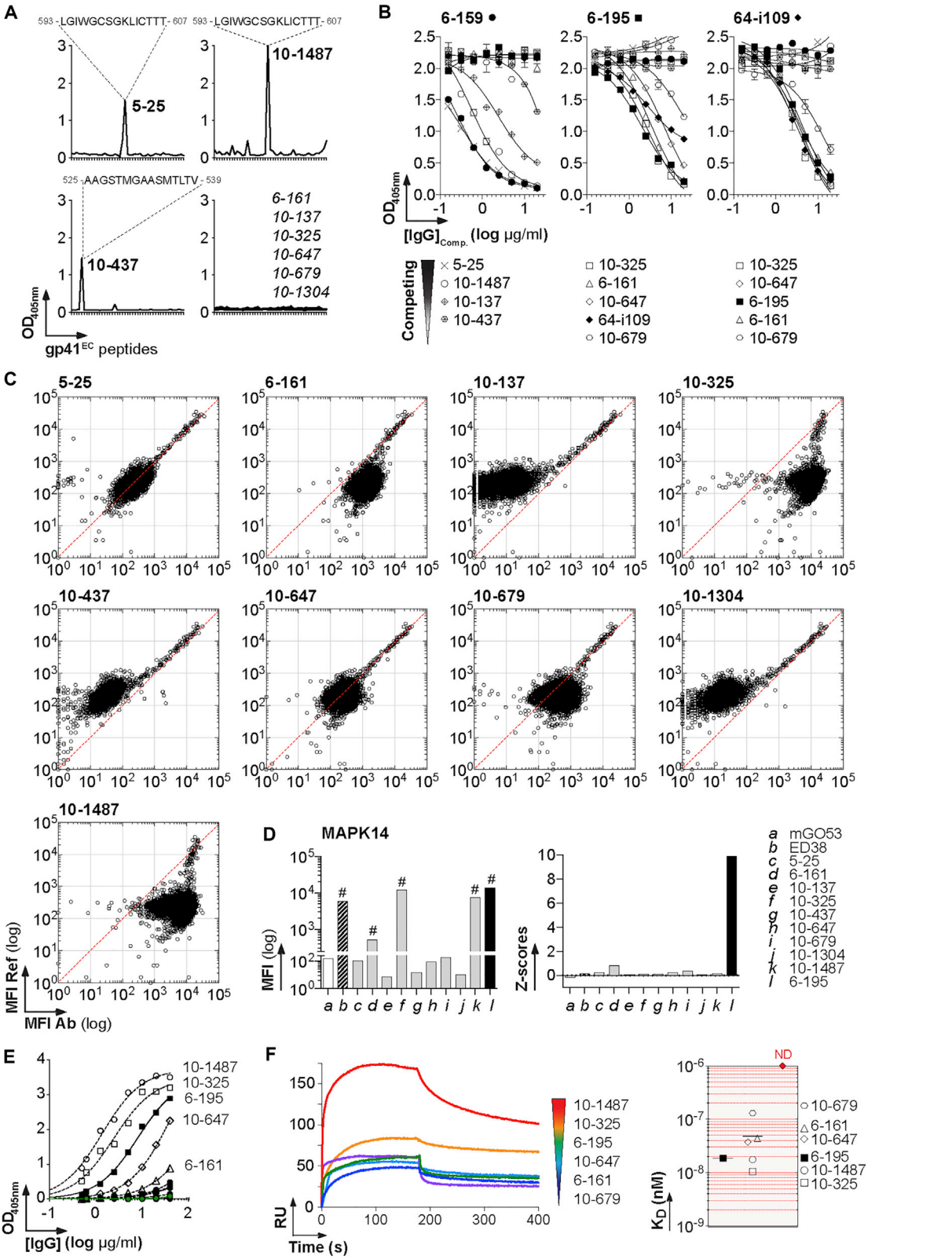

(legend on next page)

mammary gland compartments share certain B cell clones (Lindner et al., 2015), the nature, magnitude, and quality of humoral responses to HIV-1 likely differ at distinct mucosal sites.

We show that a substantial proportion of gp140-captured intestinal B cell antibodies from infected individuals reacted with low affinity to HIV-1 Env proteins. This suggests a very low frequency of high-affinity gp160 B cells in rectosigmoid tissues and, conversely, an abundance of non-HIV-1 affinity-matured and polyreactive mucosa-homing memory B cells and plasmablasts (Benckert et al., 2011; Bunker et al., 2017; Fransen et al., 2015). Alternatively, it cannot be excluded that the baiting strategy, based on the recognition of a single viral strain-derived, foldon-stabilized gp140 trimers with an ''open'' conformational state, was not fully efficient for the isolation of the entire population of high-affinity HIV-1 B cells from the gut. Interestingly, we found that HIV-1 Env glycoproteins were also weakly recognized by polyreactive and somatically mutated blood and intestinal B cell antibodies from HIV-1-naive individuals. Polyreactive antibodies bound particularly well to the gp41 moiety. This is in agreement with the works of Haynes and colleagues (Trama et al., 2014; Williams et al., 2015) showing that polyreactive and commensals-reactive B cells can cross-react with gp140, particularly the gp41 protein, even though none of the gp41-reactive antibodies described here expressed the V_H1-69 gene previously associated with mucosal gp41 antibody responses (Trama et al., 2014; Williams et al., 2015). In fact, it has been speculated that pre-activated, mutated, memory B cells residing in the gut before the infection are recruited through polyreactive binding to gp41 and ultimately mature toward HIV-1 Env. This phenomenon of ''immune diversion'' at mucosal sites could thus be responsible for the predominance of naturally and vaccine-induced gp41 antibodies toward non-neutralizing HIV-1 epitopes (Trama et al., 2014; Williams et al., 2015). Apart from polyreactivity to protein moieties, antibody cross-reactivity against glycan subunits common to the viral envelope and bacteria outer membrane could also mediate HIV-1 recognition by pre-existing gut antimicrobial B cells. The binding to mannose repeats on HIV-1 Env trimers by human blood and intestinal monoclonal antibodies targeting the *Klebsiella pneumoniae* lipopolysaccharide O3-antigen have indeed been recently reported (Rollenske et al., 2018). Besides this potential immune diversion because of pre-existing poly- and glycans-reactive B cells, other phenomena, such as germinal center fade-out, B cell dysregulation (Levesque et al., 2009), bacterial translocation, and local inflammation (Klatt et al., 2013), certainly compromise gut B cell responses in infected individuals. Ileum-resident plasmablasts and memory B cells in HIV-1-infected individuals have been shown to contain very few HIV-1-specific cells (Trama et al., 2014). ART regimen early during the acute phase may be beneficial in preserving B cell immunity at mucosal sites (Planchais et al., 2018). Interestingly, we found high-affinity gp140 antibodies more frequently in the eART donor, but studies on more donors are needed to confirm that observation.

Molecular mimicry between HIV-1 and normal human proteins was described at a serological level more than 30 years ago (Bjork, 1991; Silvestris et al., 1995). The use of HIV-1 gp160 monoclonal antibodies produced from HIV-1-infected and vaccinated individuals has allowed researchers to identify several gp120/gp41 cross-reactive epitopes in microbial and human enzymes (Liu et al., 2015; Trama et al., 2014; Williams et al., 2015; Yang et al., 2013). Similarly, we found here that mucosal anti-gp140 has the capacity to cross-react against human intracellular autoantigens SMAD2/3 transcription factors, RUFY3 protein adaptor, NDEL1 oligopeptidase, PTPN22 phosphatase, and MAPK14 kinase. That intestinal HIV-1 antibodies recognized these proteins, expressed to different degrees in circulating mononuclear cells or the gut, could be fortuitous and because of sequence and/or structural homology. The cross-reactivity to MAPK14 is intriguing because the MAPK14/p38 signaling pathway is a master regulator of various cellular activities, with some implicated in HIV-1 replication and pathogenesis, such as T cell and mucosal epithelial cell apoptosis (Furler and Uittenbogaart, 2010; Nardacci et al., 2015; Tugizov, 2016). One pathological immune consequence of $CD4^+$ T cell apoptosis is the cross-presentation of self-antigens capable of inducing autoreactive $CD8^+$ T cell responses (Rawson et al., 2007). Whether $CD4^+$ T cell apoptosis could lead to the presentation of self-antigens to B cells, including MAPK14, is currently unknown. We showed here that both blood and mucosal anti-$gp41^{HR2}$ cluster II antibodies cross-react with nanomolar affinity against MAPK14. This is particularly interesting because the circulating memory B cell repertoire to HIV-1 gp41 is largely enriched with clones targeting the $gp41^{HR2}$ (Pietzsch et al., 2010). Regrettably, because of the conformational nature of the antigenic

Figure 5. Binding of HIV-1 gp41 HR2 Antibodies to MAPK14

(A) Representative ELISA graphs show the reactivity of blood anti-gp41 antibodies against overlapping peptides covering the extracellular portion of gp41 ($gp41^{EC}$). The sequences of the peptides recognized are indicated on the top.

(B) Representative ELISA graphs show the binding of biotinylated mucosal anti-gp41 to YU-2 gp140 in the presence of potential competitor antibodies (blood-derived anti-gp41 IgG). Error bars indicate the SEM of duplicate values.

(C) Protein microarray plots show the reactivity profile of blood anti-gp140 antibodies against human proteins. For each protein spot, the mean fluorescence intensity (MFI) given by the reference (mGO53) and test antibody are depicted on the y and x axes, respectively. Each dot represents the average of duplicate array proteins. The diagonal lines indicate equal binding for reference and test antibodies.

(D) Bar graphs comparing the MFI values (Left) and *Z* scores (Right) for the binding of the selected anti-gp41 antibodies to MAPK14 immobilized on the protein array.

(E) Representative ELISA graph comparing the reactivity of blood anti-gp140 antibodies to purified MAPK14 proteins. The 6-195 and mGO53 (green) were used as positive and negative control, respectively. Error bars indicate the SEM of duplicate values.

(F) Affinity of anti-gp41 antibodies to MAPK14. (Left) Representative SPR curves comparing the binding overtime of selected anti-gp41 IgGs (at 250 nM) to purified MAPK14 immobilized on the sensor chip (250 RUs). (Right) Dot plots comparing the relative affinity (K_D) of anti-gp41 antibodies to MAPK14. No binding could be detected (ND) for the following antibodies: 5-25, 10-137, 10-437, and 10-1304.

See also Figure S6.

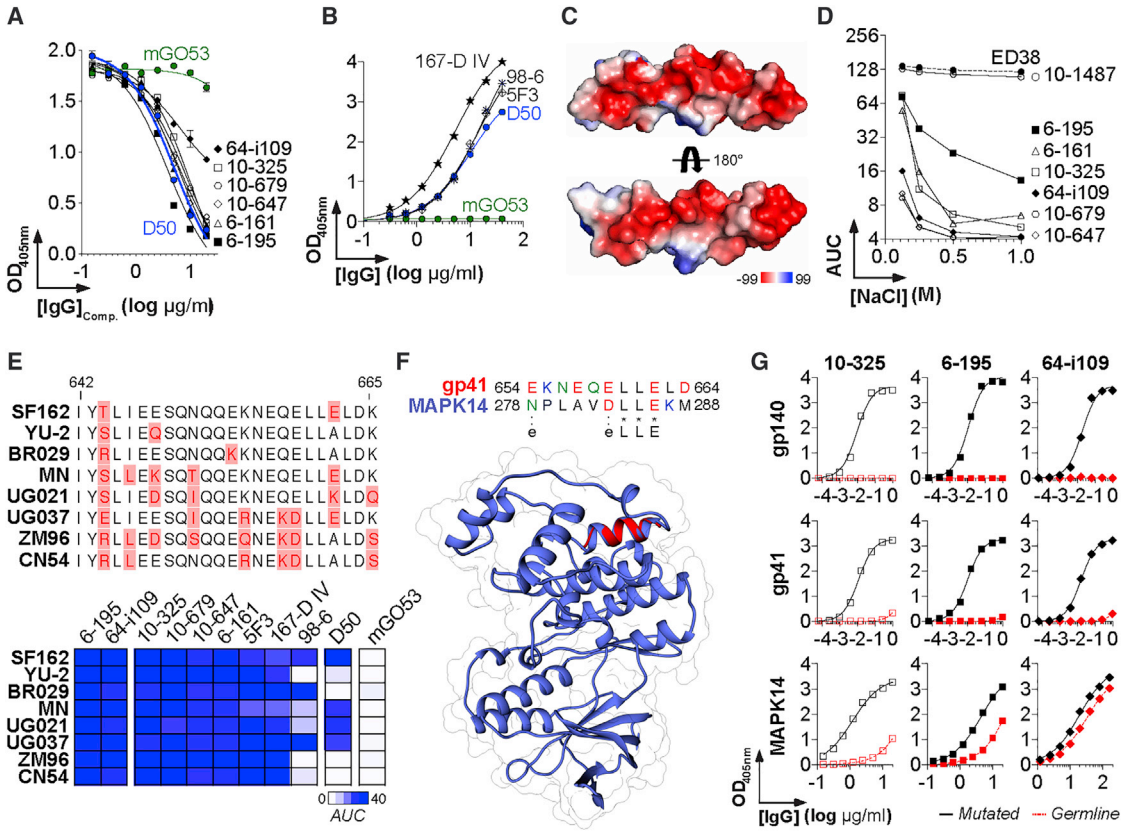

Figure 6. Interactions of Anti-HR2 Cluster II Antibodies with MAPK14

(A) Representative ELISA graph shows the binding of biotinylated anti-cluster II D50 antibody to MN gp41 in the presence of potential competitor antibodies (anti-gp41^{HR2} IgGs). mGO53 is the negative control (green).

(B) Representative ELISA graph shows the binding of murine (D50) and human (167-D IV, 98-6, and 5F3) anti-cluster II antibodies to purified MAPK14. mGO53 is the negative control (green).

(C) Surface representations show the electrostatic potentials of the gp41 cluster II (residues 642–664) (deposited in the Protein Data Base under PDB: 1ENV) calculated with PyMOL, colored blue (positive electrostatic potential) to red (negative electrostatic potential).

(D) Representative ELISA graph shows the area under the curves of $OD_{405\ nm}$ values (AUC) for the binding of the selected IgG antibodies to purified MAPK14 in presence of increasing salt concentration.

(E) (Top) Amino acid sequence alignment of the gp41 region spanning residues 642–665. Amino acid variations are shown in red. (Bottom) Heat map comparing the mean AUC values for the ELISA binding of anti-gp41 and control antibodies to the selected HIV-1 Env strains (n = 8) as measured in Figure S7. Color intensity is proportional to the reactivity level, with darker-blue colors indicating high binding, whereas light colors show moderate binding (white, no binding).

(F) Diagram shows the sequence alignment (Top) based on the structural superposition (Bottom) between a gp41^{HR2} cluster II peptide (red, from PDB: 1ENV) and MAPK14 (blue, PDB: 5ETI).

(G) ELISA graph comparing the binding of mutated anti-gp41 antibodies (black straight lines) and their germline counterparts (red dotted lines) to trimeric YU-2 gp140, gp41, and MAPK14.

Error bars in (A), (B), (D), and (G) indicate the SEM of duplicate values. See also Figure S7.

determinants recognized by anti-cluster II IgG, we could not map the targeted epitopes on both HIV-1 gp140 and MAPK14 and, therefore, could not precisely pinpoint the homology motifs. Whether these antibodies with a MAPK14-binding potential *in vivo* could have pathological effects in infected humans is unclear because MAPK14 is a cytoplasmic and nuclear protein, probably not accessible to antibodies.

Immune tolerance control would normally proscribe HIV-1 B cells reacting strongly enough with self-antigens. However, HIV-1-associated immune perturbations often lead to serum autoantibody production (Mouquet, 2014; Mouquet and Nussenzweig, 2012), suggesting that B cell tolerance mechanisms are somehow defective or relaxed in infected humans (Bonsignori et al., 2014; Mouquet, 2014; Schroeder et al., 2017). The loss of regulatory T cells and/or their anergy-prone state is certainly a key factor facilitating the emergence of autoreactive B cell clones during HIV-1 infection (Moody et al., 2016). Clones expressing a B cell receptor with a dual reactivity to HIV-1 and self-antigens could also be redeemed from tolerance purge via the selection of antibody mutations' increasing affinity to HIV-1 Env but disfavoring high autoantigen binding (Burnett et al., 2018; Kara and Nussenzweig, 2018; Kelsoe and Haynes, 2018). Accumulating data from human (Reed et al., 2016; Sabouri et al., 2014; Tan et al., 2016) and mouse models (Sabouri

et al., 2014; Burnett et al., 2018) converge toward the existence of such a "B cell redemption" mechanism, which permits the recruitment of autoreactive clones during the germinal center reaction in response to natural infection or vaccination. However, it is not clear whether HIV-1-induced chronic, antigenic stimulation and immune dysregulation would not interfere with clonal redemption mechanisms. Self-reactivity has been linked to the maturation of HIV-1-specific clones toward enhanced affinity and neutralization (Alam et al., 2009; Liao et al., 2013; Prigent et al., 2018). Mutating away from self-binding without losing optimal interactions with viral antigens may, therefore, be difficult. Because of the nature of its Env glycoproteins, recognized by both poly-reactive and cross-reactive B cells, it is, thus, tempting to speculate that HIV-1 could divert the mucosal B cell response toward the generation of poorly functional antibodies to immunodominant epitopes unable to control viral transmission and dissemination. This is an attractive scenario that demands to be further investigated.

STAR★METHODS

Detailed methods are provided in the online version of this paper and include the following:

- KEY RESOURCES TABLE
- CONTACT FOR REAGENT AND RESOURCE SHARING
- EXPERIMENTAL MODEL AND SUBJECT DETAILS
  - Human samples
- METHOD DETAILS
  - Antigens and antibody controls
  - Mucosal cells isolation and flow cytometry immunophenotyping
  - Single B cell FACS sorting and expression-cloning of antibodies
  - ELISAs
  - HIV-1 virus production and *in vitro* neutralization assay
  - *In vitro* viral transcytosis assay
  - Flow cytometry binding analysis to infected cells
  - Viral capture assay
  - ADCC assay
  - SPR binding assay
  - HEp-2 IFA
  - Protein microarray binding analyses
- QUANTIFICATION AND STATISTICAL ANALYSIS

SUPPLEMENTAL INFORMATION

Supplemental Information can be found online at https://doi.org/10.1016/j.celrep.2019.03.032.

ACKNOWLEDGMENTS

We are grateful to all HIV-infected participants who consented to be part of this study. We thank Dr. Yoann Madec (Emerging Diseases Epidemiology Unit, Institut Pasteur) for his help with the statistical analyses, Nathalie Jolly from the clinical core of the Center for Translational Sciences (CTS, Institut Pasteur) for her assistance on the preparation of the BHUANTIVIH protocol, Sandrine Schmutz and Sophie Novault for their help with single-cell sorting (CTS, Institut Pasteur), and Dr. Jagadeesh Bayry (Centre de Recherche des Cordeliers, Paris) for manuscript editing. We also thank the NIH AIDS Reagent Program (division of AIDS, NIAID, NIH) for contributing reagents and the Agence National de Recherche sur le SIDA et les hépatites virales (ANRS) for an equipment grant. Work in the O.S. lab is funded by the Institut Pasteur, ANRS, Sidaction, the Vaccine Research Institute (ANR-10-LABX-77), the Labex IBEID (ANR-10-IHUB-0002), the "TIMTAMDEN" ANR-14-CE14-0029, the "CHIKV-Viro-Immuno" ANR-14-CE14-0015-01, and the Gilead HIV Cure program. H.M. received core grants from the G5 Institut Pasteur program, the Milieu Intérieur program (ANR-10-LABX-69-01), and INSERM. This work was funded by the European Research Council (ERC)-Seventh Framework Program (ERC-2013-StG 337146). C.P., A.K., and T.H. were supported by the ERC-2013-StG 337146 program and J.P. by an ANRS postdoctoral fellowship. J.D.D. was supported by an ERC starting grant (ERC-2015-StG 678905).

AUTHOR CONTRIBUTIONS

H.M. conceived the study and designed experiments. T.P., L.L., and L.H. provided biological human samples. C.P., A. Kök, C.P., A. Kanyavuz, V.L., T.B., F.G.-B., J.P., T.H., O.S., J.D.D., L.H., and H.M. performed and analyzed the experiments. T.R. and H.W. provided the collection of expression vectors for mucosal IgG antibodies. C.P. and H.M. wrote the manuscript with contributions from all the authors.

DECLARATION OF INTERESTS

The authors declare no competing interests.

Received: June 20, 2018
Revised: February 19, 2019
Accepted: March 8, 2019
Published: April 9, 2019

REFERENCES

Alam, S.M., Morelli, M., Dennison, S.M., Liao, H.X., Zhang, R., Xia, S.M., Rits-Volloch, S., Sun, L., Harrison, S.C., Haynes, B.F., and Chen, B. (2009). Role of HIV membrane in neutralization by two broadly neutralizing antibodies. Proc. Natl. Acad. Sci. USA *106*, 20234–20239.

Astronomo, R.D., Santra, S., Ballweber-Fleming, L., Westerberg, K.G., Mach, L., Hensley-McBain, T., Sutherland, L., Mildenberg, B., Morton, G., Yates, N.L., et al. (2016). Neutralization takes precedence over IgG or IgA isotype-related functions in mucosal HIV-1 antibody-mediated protection. EBioMedicine *14*, 97–111.

Benckert, J., Schmolka, N., Kreschel, C., Zoller, M.J., Sturm, A., Wiedenmann, B., and Wardemann, H. (2011). The majority of intestinal IgA^+ and IgG^+ plasmablasts in the human gut are antigen-specific. J. Clin. Invest. *121*, 1946–1955.

Bjork, R.L., Jr. (1991). HIV-1: seven facets of functional molecular mimicry. Immunol. Lett. *28*, 91–96, discussion 97–99.

Bonsignori, M., Wiehe, K., Grimm, S.K., Lynch, R., Yang, G., Kozink, D.M., Perrin, F., Cooper, A.J., Hwang, K.K., Chen, X., et al. (2014). An autoreactive antibody from an SLE/HIV-1 individual broadly neutralizes HIV-1. J. Clin. Invest. *124*, 1835–1843.

Bruel, T., Guivel-Benhassine, F., Amraoui, S., Malbec, M., Richard, L., Bourdic, K., Donahue, D.A., Lorin, V., Casartelli, N., Noël, N., et al. (2016). Elimination of HIV-1-infected cells by broadly neutralizing antibodies. Nat. Commun. *7*, 10844.

Bruel, T., Guivel-Benhassine, F., Lorin, V., Lortat-Jacob, H., Baleux, F., Bourdic, K., Noël, N., Lambotte, O., Mouquet, H., and Schwartz, O. (2017). Lack of ADCC breadth of human nonneutralizing Anti-HIV-1 antibodies. J. Virol. *91*, e02440-16.

Buchacher, A., Predl, R., Strutzenberger, K., Steinfellner, W., Trkola, A., Purtscher, M., Gruber, G., Tauer, C., Steindl, F., Jungbauer, A., et al. (1994). Generation of human monoclonal antibodies against HIV-1 proteins; electrofusion and Epstein-Barr virus transformation for peripheral blood lymphocyte immortalization. AIDS Res. Hum. Retroviruses *10*, 359–369.

Bunker, J.J., Erickson, S.A., Flynn, T.M., Henry, C., Koval, J.C., Meisel, M., Jabri, B., Antonopoulos, D.A., Wilson, P.C., and Bendelac, A. (2017). Natural

polyreactive IgA antibodies coat the intestinal microbiota. Science *358*, eann6619.

Burnett, D.L., Langley, D.B., Schofield, P., Hermes, J.R., Chan, T.D., Jackson, J., Bourne, K., Reed, J.H., Patterson, K., Porebski, B.T., et al. (2018). Germinal center antibody mutation trajectories are determined by rapid self/foreign discrimination. Science *360*, 223–226.

Casartelli, N., Sourisseau, M., Feldmann, J., Guivel-Benhassine, F., Mallet, A., Marcelin, A.G., Guatelli, J., and Schwartz, O. (2010). Tetherin restricts productive HIV-1 cell-to-cell transmission. PLoS Pathog. *6*, e1000955.

Chaoul, N., Burelout, C., Peruchon, S., van Buu, B.N., Laurent, P., Proust, A., Raphael, M., Garraud, O., Le Grand, R., Prevot, S., and Richard, Y. (2012). Default in plasma and intestinal IgA responses during acute infection by simian immunodeficiency virus. Retrovirology *9*, 43.

Cheeseman, H.M., Olejniczak, N.J., Rogers, P.M., Evans, A.B., King, D.F., Ziprin, P., Liao, H.X., Haynes, B.F., and Shattock, R.J. (2016). Broadly neutralizing antibodies display potential for prevention of HIV-1 infection of mucosal tissue superior to that of nonneutralizing antibodies. J. Virol. *91*, e01762-16.

Cohen, Y.Z., and Caskey, M. (2018). Broadly neutralizing antibodies for treatment and prevention of HIV-1 infection. Curr. Opin. HIV AIDS *13*, 366–373.

Costiniuk, C.T., and Angel, J.B. (2012). Human immunodeficiency virus and the gastrointestinal immune system: does highly active antiretroviral therapy restore gut immunity? Mucosal Immunol. *5*, 596–604.

Dillon, S.M., Frank, D.N., and Wilson, C.C. (2016). The gut microbiome and HIV-1 pathogenesis: a two-way street. AIDS *30*, 2737–2751.

Earl, P.L., Broder, C.C., Doms, R.W., and Moss, B. (1997). Epitope map of human immunodeficiency virus type 1 gp41 derived from 47 monoclonal antibodies produced by immunization with oligomeric envelope protein. J. Virol. *71*, 2674–2684.

Fouda, G.G., Yates, N.L., Pollara, J., Shen, X., Overman, G.R., Mahlokozera, T., Wilks, A.B., Kang, H.H., Salazar-Gonzalez, J.F., Salazar, M.G., et al.; Center for HIV/AIDS Vaccine Immunology (2011). HIV-specific functional antibody responses in breast milk mirror those in plasma and are primarily mediated by IgG antibodies. J. Virol. *85*, 9555–9567.

Fransen, F., Zagato, E., Mazzini, E., Fosso, B., Manzari, C., El Aidy, S., Chiavelli, A., D'Erchia, A.M., Sethi, M.K., Pabst, O., et al. (2015). BALB/c and C57BL/6 mice differ in polyreactive IgA abundance, which impacts the generation of antigen-specific IgA and microbiota diversity. Immunity *43*, 527–540.

Friedman, J., Alam, S.M., Shen, X., Xia, S.M., Stewart, S., Anasti, K., Pollara, J., Fouda, G.G., Yang, G., Kelsoe, G., et al. (2012). Isolation of HIV-1-neutralizing mucosal monoclonal antibodies from human colostrum. PLoS ONE *7*, e37648.

Furler, R.L., and Uittenbogaart, C.H. (2010). Signaling through the P38 and ERK pathways: a common link between HIV replication and the immune response. Immunol. Res. *48*, 99–109.

Gorny, M.K., Gianakakos, V., Sharpe, S., and Zolla-Pazner, S. (1989). Generation of human monoclonal antibodies to human immunodeficiency virus. Proc. Natl. Acad. Sci. USA *86*, 1624–1628.

Horwitz, J.A., Bar-On, Y., Lu, C.L., Fera, D., Lockhart, A.A.K., Lorenzi, J.C.C., Nogueira, L., Golijanin, J., Scheid, J.F., Seaman, M.S., et al. (2017). Non-neutralizing Antibodies Alter the Course of HIV-1 Infection In Vivo. Cell *170*, 637–648.

Jeffries, T.L., Jr., Sacha, C.R., Pollara, J., Himes, J., Jaeger, F.H., Dennison, S.M., McGuire, E., Kunz, E., Eudailey, J.A., Trama, A.M., et al. (2016). The function and affinity maturation of HIV-1 gp120-specific monoclonal antibodies derived from colostral B cells. Mucosal Immunol. *9*, 414–427.

Kara, E.E., and Nussenzweig, M.C. (2018). Redemption for self-reactive antibodies. Science *360*, 152–153.

Kelsoe, G., and Haynes, B.F. (2018). What are the primary limitations in B-cell affinity maturation, and how much affinity maturation can we drive with vaccination? breaking through immunity's glass ceiling. Cold Spring Harb. Perspect. Biol. *10*, a029397.

Klatt, N.R., Funderburg, N.T., and Brenchley, J.M. (2013). Microbial translocation, immune activation, and HIV disease. Trends Microbiol. *21*, 6–13.

Kök, A., Hocqueloux, L., Hocini, H., Carrière, M., Lefrou, L., Guguin, A., Tisserand, P., Bonnabau, H., Avettand-Fenoel, V., Prazuck, T., et al. (2015). Early initiation of combined antiretroviral therapy preserves immune function in the gut of HIV-infected patients. Mucosal Immunol. *8*, 127–140.

Kubinak, J.L., and Round, J.L. (2016). Do antibodies select a healthy microbiota? Nat. Rev. Immunol. *16*, 767–774.

Levesque, M.C., Moody, M.A., Hwang, K.K., Marshall, D.J., Whitesides, J.F., Amos, J.D., Gurley, T.C., Allgood, S., Haynes, B.B., Vandergrift, N.A., et al. (2009). Polyclonal B cell differentiation and loss of gastrointestinal tract germinal centers in the earliest stages of HIV-1 infection. PLoS Med. *6*, e1000107.

Li, M., Gao, F., Mascola, J.R., Stamatatos, L., Polonis, V.R., Koutsoukos, M., Voss, G., Goepfert, P., Gilbert, P., Greene, K.M., et al. (2005). Human immunodeficiency virus type 1 env clones from acute and early subtype B infections for standardized assessments of vaccine-elicited neutralizing antibodies. J. Virol. *79*, 10108–10125.

Liao, H.X., Chen, X., Munshaw, S., Zhang, R., Marshall, D.J., Vandergrift, N., Whitesides, J.F., Lu, X., Yu, J.S., Hwang, K.K., et al. (2011). Initial antibodies binding to HIV-1 gp41 in acutely infected subjects are polyreactive and highly mutated. J. Exp. Med. *208*, 2237–2249.

Liao, H.X., Lynch, R., Zhou, T., Gao, F., Alam, S.M., Boyd, S.D., Fire, A.Z., Roskin, K.M., Schramm, C.A., Zhang, Z., et al.; NISC Comparative Sequencing Program (2013). Co-evolution of a broadly neutralizing HIV-1 antibody and founder virus. Nature *496*, 469–476.

Lindner, C., Thomsen, I., Wahl, B., Ugur, M., Sethi, M.K., Friedrichsen, M., Smoczek, A., Ott, S., Baumann, U., Suerbaum, S., et al. (2015). Diversification of memory B cells drives the continuous adaptation of secretory antibodies to gut microbiota. Nat. Immunol. *16*, 880–888.

Liu, M., Yang, G., Wiehe, K., Nicely, N.I., Vandergrift, N.A., Rountree, W., Bonsignori, M., Alam, S.M., Gao, J., Haynes, B.F., and Kelsoe, G. (2015). Polyreactivity and autoreactivity among HIV-1 antibodies. J. Virol. *89*, 784–798.

Lorin, V., and Mouquet, H. (2015). Efficient generation of human IgA monoclonal antibodies. J. Immunol. Methods *422*, 102–110.

Lorin, V., Malbec, M., Eden, C., Bruel, T., Porrot, F., Seaman, M.S., Schwartz, O., and Mouquet, H. (2017). Broadly neutralizing antibodies suppress post-transcytosis HIV-1 infectivity. Mucosal Immunol. *10*, 814–826.

Lycke, N.Y., and Bemark, M. (2017). The regulation of gut mucosal IgA B-cell responses: recent developments. Mucosal Immunol. *10*, 1361–1374.

Mabuka, J., Nduati, R., Odem-Davis, K., Peterson, D., and Overbaugh, J. (2012). HIV-specific antibodies capable of ADCC are common in breastmilk and are associated with reduced risk of transmission in women with high viral loads. PLoS Pathog. *8*, e1002739.

Meffre, E., Schaefer, A., Wardemann, H., Wilson, P., Davis, E., and Nussenzweig, M.C. (2004). Surrogate light chain expressing human peripheral B cells produce self-reactive antibodies. J. Exp. Med. *199*, 145–150.

Mehandru, S., Poles, M.A., Tenner-Racz, K., Horowitz, A., Hurley, A., Hogan, C., Boden, D., Racz, P., and Markowitz, M. (2004). Primary HIV-1 infection is associated with preferential depletion of CD4+ T lymphocytes from effector sites in the gastrointestinal tract. J. Exp. Med. *200*, 761–770.

Meng, E.C., Pettersen, E.F., Couch, G.S., Huang, C.C., and Ferrin, T.E. (2006). Tools for integrated sequence-structure analysis with UCSF Chimera. BMC Bioinformatics *7*, 339.

Moody, M.A., Pedroza-Pacheco, I., Vandergrift, N.A., Chui, C., Lloyd, K.E., Parks, R., Soderberg, K.A., Ogbe, A.T., Cohen, M.S., Liao, H.X., et al. (2016). Immune perturbations in HIV-1-infected individuals who make broadly neutralizing antibodies. Sci. Immunol. *1*, aag0851.

Mouquet, H. (2014). Antibody B cell responses in HIV-1 infection. Trends Immunol. *35*, 549–561.

Mouquet, H., and Nussenzweig, M.C. (2012). Polyreactive antibodies in adaptive immune responses to viruses. Cell. Mol. Life Sci. *69*, 1435–1445.

Mouquet, H., Farci, S., Joly, P., Maillère, B., Leblond, J., Drouot, L., Leprince, J., Tonon, M.C., Loiseau, P., Charron, D., et al. (2006). A truncated alternative spliced isoform of human desmoglein 1 contains a specific T cell epitope

binding to the pemphigus foliaceus-associated HLA class II DRβ1*0102 molecule. J. Immunol. *177*, 6517–6526.

Mouquet, H., Klein, F., Scheid, J.F., Warncke, M., Pietzsch, J., Oliveira, T.Y., Velinzon, K., Seaman, M.S., and Nussenzweig, M.C. (2011). Memory B cell antibodies to HIV-1 gp140 cloned from individuals infected with clade A and B viruses. PLoS ONE *6*, e24078.

Mouquet, H., Scharf, L., Euler, Z., Liu, Y., Eden, C., Scheid, J.F., Halper-Stromberg, A., Gnanapragasam, P.N., Spencer, D.I., Seaman, M.S., et al. (2012). Complex-type N-glycan recognition by potent broadly neutralizing HIV antibodies. Proc. Natl. Acad. Sci. USA *109*, E3268–E3277.

Nardacci, R., Perfettini, J.L., Grieco, L., Thieffry, D., Kroemer, G., and Piacentini, M. (2015). Syncytial apoptosis signaling network induced by the HIV-1 envelope glycoprotein complex: an overview. Cell Death Dis. *6*, e1846.

Ochsenbauer, C., Edmonds, T.G., Ding, H., Keele, B.F., Decker, J., Salazar, M.G., Salazar-Gonzalez, J.F., Shattock, R., Haynes, B.F., Shaw, G.M., et al. (2012). Generation of transmitted/founder HIV-1 infectious molecular clones and characterization of their replication capacity in CD4 T lymphocytes and monocyte-derived macrophages. J. Virol. *86*, 2715–2728.

Pietzsch, J., Scheid, J.F., Mouquet, H., Seaman, M.S., Broder, C.C., and Nussenzweig, M.C. (2010). Anti-gp41 antibodies cloned from HIV-infected patients with broadly neutralizing serologic activity. J. Virol. *84*, 5032–5042.

Planchais, C., Hocqueloux, L., Ibanez, C., Gallien, S., Copie, C., Surenaud, M., Kok, A., Lorin, V., Fusaro, M., Delfau-Larue, M.H., et al. (2018). Early antiretroviral therapy preserves functional follicular helper T and HIV-specific B cells in the gut mucosa of HIV-1-infected individuals. J. Immunol. *200*, 3519–3529.

Ponte, R., Mehraj, V., Ghali, P., Couëdel-Courteille, A., Cheynier, R., and Routy, J.P. (2016). Reversing gut damage in HIV infection: using non-human primate models to instruct clinical research. EBioMedicine *4*, 40–49.

Prigent, J., Lorin, V., Kök, A., Hieu, T., Bourgeau, S., and Mouquet, H. (2016). Scarcity of autoreactive human blood IgA^+ memory B cells. Eur. J. Immunol. *46*, 2340–2351.

Prigent, J., Jarossay, A., Planchais, C., Eden, C., Dufloo, J., Kök, A., Lorin, V., Vratskikh, O., Couderc, T., Bruel, T., et al. (2018). Conformational plasticity in broadly neutralizing HIV-1 antibodies triggers polyreactivity. Cell Rep. *23*, 2568–2581.

Rawson, P.M., Molette, C., Videtta, M., Altieri, L., Franceschini, D., Donato, T., Finocchi, L., Propato, A., Paroli, M., Meloni, F., et al. (2007). Cross-presentation of caspase-cleaved apoptotic self antigens in HIV infection. Nat. Med. *13*, 1431–1439.

Reed, J.H., Jackson, J., Christ, D., and Goodnow, C.C. (2016). Clonal redemption of autoantibodies by somatic hypermutation away from self-reactivity during human immunization. J. Exp. Med. *213*, 1255–1265.

Richard, J., Prévost, J., Alsahafi, N., Ding, S., and Finzi, A. (2018). Impact of HIV-1 envelope conformation on ADCC responses. Trends Microbiol. *26*, 253–265.

Rollenske, T., Szijarto, V., Lukasiewicz, J., Guachalla, L.M., Stojkovic, K., Hartl, K., Stulik, L., Kocher, S., Lasitschka, F., Al-Saeedi, M., et al. (2018). Cross-specificity of protective human antibodies against *Klebsiella pneumoniae* LPS O-antigen. Nat. Immunol. *19*, 617–624.

Sabouri, Z., Schofield, P., Horikawa, K., Spierings, E., Kipling, D., Randall, K.L., Langley, D., Roome, B., Vazquez-Lombardi, R., Rouet, R., et al. (2014). Redemption of autoantibodies on anergic B cells by variable-region glycosylation and mutation away from self-reactivity. Proc. Natl. Acad. Sci. USA *111*, E2567–E2575.

Sacha, C.R., Vandergrift, N., Jeffries, T.L., Jr., McGuire, E., Fouda, G.G., Liebl, B., Marshall, D.J., Gurley, T.C., Stiegel, L., Whitesides, J.F., et al. (2015). Restricted isotype, distinct variable gene usage, and high rate of gp120 specificity of HIV-1 envelope-specific B cells in colostrum compared with those in blood of HIV-1-infected, lactating African women. Mucosal Immunol. *8*, 316–326.

Santra, S., Tomaras, G.D., Warrier, R., Nicely, N.I., Liao, H.X., Pollara, J., Liu, P., Alam, S.M., Zhang, R., Cocklin, S.L., et al. (2015). Human non-neutralizing HIV-1 envelope monoclonal antibodies limit the number of founder viruses during SHIV mucosal infection in rhesus macaques. PLoS Pathog. *11*, e1005042.

Sarzotti-Kelsoe, M., Daniell, X., Todd, C.A., Bilska, M., Martelli, A., LaBranche, C., Perez, L.G., Ochsenbauer, C., Kappes, J.C., Rountree, W., et al. (2014). Optimization and validation of a neutralizing antibody assay for HIV-1 in A3R5 cells. J. Immunol. Methods *409*, 147–160.

Scheid, J.F., Mouquet, H., Feldhahn, N., Seaman, M.S., Velinzon, K., Pietzsch, J., Ott, R.G., Anthony, R.M., Zebroski, H., Hurley, A., et al. (2009). Broad diversity of neutralizing antibodies isolated from memory B cells in HIV-infected individuals. Nature *458*, 636–640.

Scheid, J.F., Mouquet, H., Ueberheide, B., Diskin, R., Klein, F., Oliveira, T.Y., Pietzsch, J., Fenyo, D., Abadir, A., Velinzon, K., et al. (2011). Sequence and structural convergence of broad and potent HIV antibodies that mimic CD4 binding. Science *333*, 1633–1637.

Schroeder, K.M.S., Agazio, A., Strauch, P.J., Jones, S.T., Thompson, S.B., Harper, M.S., Pelanda, R., Santiago, M.L., and Torres, R.M. (2017). Breaching peripheral tolerance promotes the production of HIV-1-neutralizing antibodies. J. Exp. Med. *214*, 2283–2302.

Silvestris, F., Williams, R.C., Jr., and Dammacco, F. (1995). Autoreactivity in HIV-1 infection: the role of molecular mimicry. Clin. Immunol. Immunopathol. *75*, 197–205.

Spencer, J., and Sollid, L.M. (2016). The human intestinal B-cell response. Mucosal Immunol. *9*, 1113–1124.

Tan, J., Pieper, K., Piccoli, L., Abdi, A., Perez, M.F., Geiger, R., Tully, C.M., Jarrossay, D., Maina Ndungu, F., Wambua, J., et al. (2016). A LAIR1 insertion generates broadly reactive antibodies against malaria variant antigens. Nature *529*, 105–109.

Tiller, T., Meffre, E., Yurasov, S., Tsuiji, M., Nussenzweig, M.C., and Wardemann, H. (2008). Efficient generation of monoclonal antibodies from single human B cells by single cell RT-PCR and expression vector cloning. J. Immunol. Methods *329*, 112–124.

Trama, A.M., Moody, M.A., Alam, S.M., Jaeger, F.H., Lockwood, B., Parks, R., Lloyd, K.E., Stolarchuk, C., Scearce, R., Foulger, A., et al. (2014). HIV-1 envelope gp41 antibodies can originate from terminal ileum B cells that share cross-reactivity with commensal bacteria. Cell Host Microbe *16*, 215–226.

Tudor, D., Derrien, M., Diomede, L., Drillet, A.S., Houimel, M., Moog, C., Reynes, J.M., Lopalco, L., and Bomsel, M. (2009). HIV-1 gp41-specific monoclonal mucosal IgAs derived from highly exposed but IgG-seronegative individuals block HIV-1 epithelial transcytosis and neutralize CD4(+) cell infection: an IgA gene and functional analysis. Mucosal Immunol. *2*, 412–426.

Tugizov, S. (2016). Human immunodeficiency virus-associated disruption of mucosal barriers and its role in HIV transmission and pathogenesis of HIV/AIDS disease. Tissue Barriers *4*, e1159276.

Wardemann, H., Yurasov, S., Schaefer, A., Young, J.W., Meffre, E., and Nussenzweig, M.C. (2003). Predominant autoantibody production by early human B cell precursors. Science *301*, 1374–1377.

Williams, W.B., Liao, H.X., Moody, M.A., Kepler, T.B., Alam, S.M., Gao, F., Wiehe, K., Trama, A.M., Jones, K., Zhang, R., et al. (2015). HIV-1 VACCINES. Diversion of HIV-1 vaccine-induced immunity by gp41-microbiota cross-reactive antibodies. Science *349*, aab1253.

Xu, J.Y., Gorny, M.K., Palker, T., Karwowska, S., and Zolla-Pazner, S. (1991). Epitope mapping of two immunodominant domains of gp41, the transmembrane protein of human immunodeficiency virus type 1, using ten human monoclonal antibodies. J. Virol. *65*, 4832–4838.

Yang, G., Holl, T.M., Liu, Y., Li, Y., Lu, X., Nicely, N.I., Kepler, T.B., Alam, S.M., Liao, H.X., Cain, D.W., et al. (2013). Identification of autoantigens recognized by the 2F5 and 4E10 broadly neutralizing HIV-1 antibodies. J. Exp. Med. *210*, 241–256.

Yates, N.L., Stacey, A.R., Nolen, T.L., Vandergrift, N.A., Moody, M.A., Montefiori, D.C., Weinhold, K.J., Blattner, W.A., Borrow, P., Shattock, R., et al. (2013). HIV-1 gp41 envelope IgA is frequently elicited after transmission but has an initial short response half-life. Mucosal Immunol. *6*, 692–703.

STAR★METHODS

KEY RESOURCES TABLE

REAGENT or RESOURCE	SOURCE	IDENTIFIER
Antibodies		
Human monoclonal IgG PGT128	Mouquet et al., 2012	N/A
Human monoclonal IgG 10-1074	Mouquet et al., 2012	N/A
Human monoclonal IgG 3BNC117	Scheid et al., 2011	N/A
Human monoclonal IgG 5-25	Scheid et al., 2009	N/A
Human monoclonal IgG 6-161	Scheid et al., 2009	N/A
Human monoclonal IgG 6-161 GL	This paper	N/A
Human monoclonal IgG 10-137	Mouquet et al., 2011	N/A
Human monoclonal IgG 10-325	Mouquet et al., 2011	N/A
Human monoclonal IgG 10-437	Mouquet et al., 2011	N/A
Human monoclonal IgG 10-647	Mouquet et al., 2011	N/A
Human monoclonal IgG 10-679	Mouquet et al., 2011	N/A
Human monoclonal IgG 10-1304	Mouquet et al., 2011	N/A
Human monoclonal IgG 10-1487	Mouquet et al., 2011	N/A
Human monoclonal IgG/IgA 6-195	This paper	N/A
Human monoclonal IgG 6-195 GL	This paper	N/A
Human monoclonal IgG 64-i109	This paper	N/A
Human monoclonal IgG 64-i109 GL	This paper	N/A
Human monoclonal IgG 18-295	This paper	N/A
Human monoclonal IgG ED38	Meffre et al., 2004	N/A
Human monoclonal IgG mGO53	Wardemann et al., 2003	N/A
Mouse monoclonal IgG D50	Earl et al., 1997; NIH AIDS Reagent Program	Cat#11393
Human monoclonal IgG/IgA 6-159	This paper	N/A
Human monoclonal IgG 6-104	This paper	N/A
Human monoclonal IgG 558-2	Liao et al., 2011	N/A
Human monoclonal IgG DH308	Trama et al., 2014	N/A
Human monoclonal IgG DH307	Trama et al., 2014	N/A
Human monoclonal IgG 167-D IV	Xu et al., 1991, NIH AIDS Reagent Program	Cat#11681
Human monoclonal IgG 98-6	Gorny et al., 1989, NIH AIDS Reagent Program	Cat#1240
Human monoclonal IgG 5F3	Buchacher et al., 1994, NIH AIDS Reagent Program	Cat#6882
Mouse anti-human CD38-APC (HIT2)	BD biosciences	Cat#555462
Mouse anti-human CD21 BV421 (B-ly4)	BD biosciences	Cat#562966
Mouse anti-human CD27 PE-CF594 (M-T271)	BD biosciences	Cat#562297
Mouse anti-human CD19 Alexa Fluor 700 (HIB19)	BD biosciences	Cat#557921
Mouse anti-human CD24 PE-Cy7 (ML5)	BD biosciences	Cat#561646
Mouse anti-human CD10 BV650 (HI10a)	BD biosciences	Cat#563734
Mouse anti-human IgD APC-H7 (IA6-2)	BD biosciences	Cat#561305
Mouse anti-human IgM BV605 (G20-127)	BD biosciences	Cat#562977
Mouse anti-human IgG BV786 (G18-145)	BD biosciences	Cat#564230
Mouse anti-human CD138 BV711 (MI15)	BD biosciences	Cat#563184

(*Continued on next page*)

Continued

REAGENT or RESOURCE	SOURCE	IDENTIFIER
Mouse anti-human IgA FITC (IS11-8E10)	Miltenyi Biotec	Cat#130-113-475
Goat anti-human IgG Alexa Fluor 647	Life technologies	Cat#A-21445
Peroxidase AffiniPure Goat Anti-Human IgG, Fcγ fragment specific	Jackson ImmunoReseach	Cat#109-035-098
Peroxidase AffiniPure Goat Anti-Human IgA/IgG/IgM (H+L)	Jackson ImmunoReseach	Cat#109-035-064
Blood human monoclonal IgGs from healthy individuals (hd2 & hd4)	Prigent et al., 2016	N/A
Intestinal human monoclonal IgGs from healthy individuals (e.g., HD1a361 and HD2a57)	Benckert et al., 2011	N/A
Bacterial and Virus Strains		
NEB 10-beta Competent *E.coli*	New England Biolabs	C3019H
Lab adapted HIV-1 virus (NLAD8)	NIH AIDS Reagent Program	Cat#11346
Lab adapted HIV-1 virus (NL4.3)	NIH AIDS Reagent Program	Cat#7407
Lab adapted HIV-1 virus (YU-2)	NIH AIDS Reagent Program	Cat#1350
Transmitted/founder HIV-1 virus (WITO)	NIH AIDS Reagent Program	Cat#11739
Transmitted/founder HIV-1 virus (CH058)	NIH AIDS Reagent Program	Cat#11856
Transmitted/founder HIV-1 virus (CH077)	NIH AIDS Reagent Program	Cat#11742
Transmitted/founder HIV-1 virus (CH0106)	NIH AIDS Reagent Program	Cat#11743
Transmitted/founder HIV-1 virus (REJO)	NIH AIDS Reagent Program	Cat#11746
Transmitted/founder HIV-1 virus (RHPA)	NIH AIDS Reagent Program	Cat#11744
Biological Samples		
Colorectal biopsies from HIV-1^{+} individuals	Centre Hospitalier Regional d'Orléans, France	N/A
Peripheral blood mononuclear cells (PBMCs) & sera from HIV-1^{+} individuals	Centre Hospitalier Regional d'Orléans, France	N/A
Chemicals, Peptides, and Recombinant Proteins		
AviTagged clade B YU-2 gp140 trimers	Scheid et al., 2009	N/A
YU-2 gp120	Scheid et al., 2009	N/A
YU-2 gp120^{D368R}	Scheid et al., 2009	N/A
YU-2 gp120^{I420R}	Scheid et al., 2009	N/A
Clade B HXBc2 gp120^{core} proteins	Scheid et al., 2009	N/A
Clade B MN gp41 protein	NIH AIDS Reagent Program	Cat#12027
Clade B SF162 trimeric gp140	NIH AIDS Reagent Program	Cat#12026
Clade D UG021 trimeric gp140	NIH AIDS Reagent Program	Cat#12065
Clade A UG037 trimeric gp140	NIH AIDS Reagent Program	Cat#12063
Clade F BR029 trimeric gp140	NIH AIDS Reagent Program	Cat#12066
Clade C/B' CN54 trimeric gp140	NIH AIDS Reagent Program	Cat#12064
Clade C ZM96 trimeric gp140	Prigent et al., 2018	N/A
Consensus clade B 15-mer overlapping peptide library	NIH AIDS Reagent Program	Cat#9480
E. coli RNA polymerase α subunit (RNApol α)	This paper	N/A
Human recombinant MAPK14 (p38 α)	BPS Bioscience	Cat#40070
Recombinant human mucin 2	MyBioSource	Cat#MBS958652
Purified double stranded (ds)-DNA	Sigma-Aldrich	Cat#D1501
Purified Hemocyanin - Keyhole Limpet (KLH)	Sigma-Aldrich	Cat#H8283
Purified Lipopolysaccharides (LPS)	Sigma-Aldrich	Cat#L2637
Purified Insulin	Sigma-Aldrich	Cat#I9278

(*Continued on next page*)

Continued

REAGENT or RESOURCE	SOURCE	IDENTIFIER
FITC-labeled DEAE-dextran	Molecular Probes	Cat#95648
Peroxidase-conjugated streptavidin	BD Biosciences	Cat#554066
Polyethylenimine	Polysciences	23966-2
LIVE/DEAD fixable aqua dead cell stain kit	Thermo Fisher Scientific	Cat#L34957
SuperScript IV reverse transcriptase	Thermo Fisher Scientific	Cat#18091200
ReadiUse ABTS Substrate Solution	Euromedex	Cat#11001-AAT
Streptavidin R-PE conjugate	Thermo Fisher Scientific	Cat#SA10041
Critical Commercial Assays		
EZ-Link Sulfo-NHS-LC-Biotinylation kit	Thermo Fisher Scientific	Cat#21435
BirA biotin-protein ligase bulk reaction kit	Avidity, LLC	Cat#bulk BirA
HIV-1 p24 Antigen Capture Assay	Advanced Bioscience Laboratories Inc	Cat#5421
Amine Coupling Kit	Biacore, GE Healthcare	Cat# BR100050
ANA HEp-2 AeskuSlides®	Aesku.Diagnostics	Cat#51.100
FUGENE-6 transfection reagent	Promega	Cat# E2691
Experimental Models: Cell Lines		
TZM-bl cells	NIH AIDS Reagent Program	Cat# 8129
Epithelial monolayer-forming human endometrial carcinoma type A HEC-1A cells	ATCC®	Cat# HTB-112
Freestyle 293-F cells	Thermo Fisher Scientific	Cat#R79007
CEM.NKR CCR5^{+} cells	NIH AIDS Reagent Program	Cat#4376
Oligonucleotides		
IgH PCR primers	Wardemann et al., 2003; Tiller et al., 2008; Benckert et al., 2011	N/A
IgK PCR primers	Wardemann et al., 2003; Tiller et al., 2008	N/A
IgL PCR primers	Wardemann et al., 2003; Tiller et al., 2008	N/A
Recombinant DNA		
pSG3ΔEnv vector	NIH AIDS Reagent Program	Cat#11051
pcDNA3.1/Zeo$^{(+)}$ expression vector	Thermo Fisher Scientific	Cat#V86020
HIV-1 Env Expression Vector (Bal.26)	NIH AIDS Reagent Program	Cat#11446
HIV-1 Env Expression Vector (6535.3)	NIH AIDS Reagent Program	Cat#11017
HIV-1 Env Expression Vector (YU-2)	NIH AIDS Reagent Program	Cat#12133
HIV-1 Env Expression Vector (SC422661.8)	NIH AIDS Reagent Program	Cat# 11058
HIV-1 Env Expression Vector (PVO.4)	NIH AIDS Reagent Program	Cat# 11022
Software and Algorithms		
GraphPad Prism software (v6.0a)	GraphPad Prism Inc.	https://www.graphpad.com/
FlowJo software (v10.3)	FlowJo LLC	https://www.flowjo.com/solutions/flowjo
BIAevaluation software (v4.1.1)	Biacore, GE Healthcare	https://www.biacore.com/lifesciences/service/downloads/software_licenses/biaevaluation/
UCSF Chimera software (v1.9)	Meng et al., 2006	https://www.cgl.ucsf.edu/chimera/download.html
ZEN imaging software (Zen 2.0 blue version)	Zeiss	https://www.zeiss.com/microscopy/int/products/microscope-software/zen-lite/zen-lite-response.html
Spotxel® software	SICASYS Software GmbH	https://www.sicasys.de/spotxel/

(*Continued on next page*)

Continued

REAGENT or RESOURCE	SOURCE	IDENTIFIER
ProtoArray® Prospector software (v5.2.3)	Thermo Fisher Scientific	https://www.thermofisher.com/us/en/home/life-science/protein-biology/protein-assays-analysis/protein-microarrays/technical-resources/data-analysis.html.
GenePix Pro 6.0 software	Molecular Devices	http://mdc.custhelp.com/app/answers/detail/a_id/18691/~/genepix%C2%AE-pro-6-microarray-acquisition-%26-analysis-software-download-page
Other		
CM5 chips	Biacore, Inc.	BR-1000-12
Peptide M-coupled agarose beads	Invivogen	Cat#gel-pdm-5
Protein G Sepharose 4 fast flow beads	GE Healthcare	Cat#17061805
HisPur Cobalt agarose beads	Thermo Fisher Scientific	Cat#25228
ProtoArray Human Protein Microarrays	Thermo Fisher Scientific	Cat#PAH0525101
Superdex® 200 increase 10/300 GL column	GE Healthcare	Cat#GE28-9909-44

CONTACT FOR REAGENT AND RESOURCE SHARING

Further information and requests for resources and reagents should be directed to and will be fulfilled by the Lead Contact, Dr. Hugo Mouquet (hugo.mouquet@pasteur.fr).

EXPERIMENTAL MODEL AND SUBJECT DETAILS

Human samples

Samples were obtained as part of the BHUANTIVIH research protocol performed in accordance with and after ethical approval from all the French legislation and regulation authorities. Peripheral blood mononuclear cells (PBMC), sera and colon biopsies (collected by retroscopy procedure) were obtained from HIV-1 infected patients at the Centre Hospitalier Regional d'Orléans. Five HIV^+ donors (4 males and 1 female) with a median age of 48 years (range, 27-55 years) were included in the study, and were either untreated (n = 1) or treated by ART (n = 4) at the time of the blood/colon sampling. The HIV status and main clinical characteristics of the donors are summarized in Table S1. The clinical research protocol received approval from the *Comité Consultatif pour le Traitement de l'Information en matière de Recherche dans le domaine de la Santé* (CCTIRS) on December 12th 2013, the *Commission Nationale de l'Informatique et des Libertés* (CNIL) on August 8th 2014 and the *Comité de Protection des Personnes de Tours* (CPP Région Centre-Ouest 1) on December 17th 2014. All donors gave written consent to participate in this study, and data were collected under pseudo-anonymized conditions using subject coding. Ethical issues have been monitored by the Ethics Board for European contracts, an *ad hoc* independent Ethics Committee in charge of reviewing periodically sensitive ethical issues in EU funded researches when requested by the EU.

METHOD DETAILS

Antigens and antibody controls

HIV-1 antigens: AviTagged clade B YU-2 gp140 trimers, YU-2 gp120, YU-2 $gp120^{D368R}$, YU-2 $gp120^{I420R}$, clade B HXBc2 $gp120^{core}$ proteins (Scheid et al., 2009), and clade C ZM96 trimeric gp140 (Prigent et al., 2018) were produced by transient transfection of exponentially growing Freestyle 293-F suspension cells (Thermo Fisher Scientific, Waltham, MA) using polyethylenimine (PEI)-precipitation method, purified by affinity chromatography using HisPur Cobalt agarose beads (Fisher Scientific), and controlled for purity by SDS-PAGE and NativePAGE gel staining as previously described (Lorin and Mouquet, 2015; Tiller et al., 2008). The trimeric state of purified YU-2 gp140 was further confirmed by size exclusion FPLC-chromatography using an AKTA pure FPLC instrument (GE Healthcare) with a Superdex® 200 increase 10/300 GL column (GE Healthcare). YU-2 trimers used for B cell FACS capture were biotinylated using BirA biotin-protein ligase bulk reaction kit (Avidity, LLC). Purified clade B MN gp41 protein (#12027), SF162 (#12026), UG021 (#12065), UG037 (#12063), BR029 (#12066), CN54 (#12064) gp140 trimers and consensus clade B 15-mer overlapping peptide library (#9480) were provided by the NIH AIDS Reagent Program (Germantown, MD). The *E. coli* RNA polymerase α subunit (RNApol α) was produced and purified as described above for HIV-1 proteins using a codon-optimized DNA fragment (containing nucleotide sequences encoding the IgK leader peptide, the RNApol α, and an hexahistidine tag) cloned into $pcDNA3.1/Zeo^{(+)}$ expression vector.

Human HIV-1 antibodies are as follow: bNAbs anti-V3/glycans PGT128 and 10-1074 (Mouquet et al., 2012), anti-CD4bs 3BNC117 (Scheid et al., 2011), and 13 previously characterized anti-gp41 antibodies (Liao et al., 2011; Mouquet et al., 2011; Scheid et al., 2009; Trama et al., 2014). Non-HIV-1 antibodies include polyreactive and non-polyreactive antibody ED38 (Meffre et al., 2004) and mGO53 (Wardemann et al., 2003), respectively; healthy individuals' blood (from hd2 and hd4 donors [Prigent et al., 2016]) and polyreactive mucosal (from HD1-3 donors, Benckert et al. [2011]) monoclonal IgGs. Recombinant IgG antibodies were produced by co-transfection of Freestyle 293-F cells (Thermo Fisher Scientific, Waltham, MA) using PEI-precipitation method as previously described (Lorin and Mouquet, 2015; Tiller et al., 2008), and purified by affinity chromatography using protein G Sepharose 4 fast flow beads (GE Healthcare). Purified antibodies were biotinylated using the EZ-Link Sulfo-NHS-Biotin kit (Thermo Fisher Scientific). Anti-gp41^{HR2} monoclonal antibodies previously generated from immunized mice (D50 (Earl et al., 1997), #11393), and from HIV-seropositive subjects (167-D IV (Xu et al., 1991), #11681; 98-6 (Gorny et al., 1989), #1240; and 5F3 (Buchacher et al., 1994), #6882) were obtained through the NIH AIDS Reagent Program (Germantown, MD).

Mucosal cells isolation and flow cytometry immunophenotyping

Intraepithelial lymphocytes (IEL) were isolated by two rounds of vigorous shaking in DMEM-Glutamax (GIBCO, Thermo Fisher Scientific) supplemented with 1% Fetal Bovine Serum (FBS) (GIBCO), 1mM EGTA and 1.5 mM $MgCl_2$. Lamina propria lymphocytes (LPL) were isolated by two rounds of tissue digestion in medium containing collagenase II 100U/ml (Sigma, Saint-Louis, MO), followed by mechanical disruption with a syringe equipped with an 16-gauge blunt-end needle. Both IEL and LPL were washed in DMEM - Glutamax (GIBCO) supplemented with 10% FBS (GIBCO), 1% penicillin and 1% streptomycin (GIBCO). Cells were then stained for flow cytometry analyses and single-cell sorted as follow. Cells were first stained using LIVE/DEAD fixable dead cell stain kit (405 nm excitation) (Molecular Probes, Thermo Fisher Scientific) to exclude dead cells. Cells were then incubated for 30 min at 4°C with biotinylated recombinant YU2 gp140 trimers (Mouquet et al., 2011; Scheid et al., 2011). Cells were washed once with 1% FBS-PBS (FACS buffer), and incubated for 30 min at 4°C with a cocktail of mouse anti-human antibodies: CD19 A700 (HIB19, BD Biosciences, San Jose, CA), CD38 APC (HIT2, BD Biosciences), CD21 BV421 (B-ly4, BD Biosciences), CD27 PE-CF594 (M-T271, BD Biosciences), CD24 PE-Cy7 (ML5, BD Biosciences), CD10 BV650 (HI10a, BD Biosciences), IgD APC-H7 (IA6-2, BD Biosciences), IgM BV605 (G20-127, BD Biosciences), IgG BV786 (G18-145, BD Biosciences), CD138 BV711 (MI15, BD Biosciences), IgA FITC (IS11-8E10, Miltenyi Biotec, Bergisch Gladbach, Germany), and streptavidin R-PE conjugate (Invitrogen, Thermo Fisher Scientific). Finally, cells were washed with FACS buffer and resuspended in 1mM EDTA FACS buffer. Following a lymphocyte and single cell gating, live cells were gated on $CD19^+$ B cells. FACS analyses were performed using a FACS Aria II cytometer (BD Biosciences) and FlowJo software (v10.3, FlowJo LLC, Ashland, OR).

Single B cell FACS sorting and expression-cloning of antibodies

Single $CD19^+IgA^+$ and $CD19^+IgG^+$ B cells were identified as described above and sorted into 96-well PCR plates using a FACS Aria III sorter (Becton Dickinson, Franklin Lakes, NJ) as previously described (Tiller et al., 2008). Single-cell cDNA synthesis using SuperScript IV reverse transcriptase (Thermo Fisher Scientific) followed by nested-PCR amplifications of IgH, Igκ and Igλ genes, and sequences analyses for Ig gene features were performed as previously described (Tiller et al., 2008). For the reversion to germline (GL) of the selected anti-gp41 antibodies, sequences were constructed by replacing the mutated V_H-(D_H)-J_H and V_L-J_L gene segments with their GL counterparts as previously described (Mouquet et al., 2012). Purified digested PCR products were cloned into human Igγ_1-, Igα_1-, Igα_2-, Igκ- or Igλ-expressing vectors as previously described (Lorin and Mouquet, 2015; Tiller et al., 2008). Recombinant antibodies were produced by transient co-transfection of Freestyle 293-F suspension cells (Thermo Fisher Scientific) using PEI-precipitation method as previously described (Lorin and Mouquet, 2015; Tiller et al., 2008). Recombinant human antibodies and serum IgG from HIV-1 donors were purified by batch/gravity-flow affinity chromatography using peptide M-coupled agarose (Invivogen, San Diego, CA) and protein G Sepharose 4 fast flow beads (GE Healthcare, Chicago, IL) for IgAs and IgGs, respectively. Mucosal gp140 antibodies were biotinylated as described above.

ELISAs

Antibody bindings to HIV-1 envelope antigens and human mucin 2 were measured as previously described (Mouquet et al., 2011; Mouquet et al., 2012): high-binding 96-well ELISA plates (Costar, Corning) were coated overnight with 125 ng/well of purified HIV-1 envelope proteins or purified recombinant human mucin 2 (MyBioSource, Inc., San Diego, CA). After washings, plates were blocked 2 h with 2% BSA, 1mM EDTA, 0.05% Tween 20-PBS (Blocking buffer), washed, and incubated with serially diluted IgG/IgA antibodies and serum IgG in PBS for HIV-1 proteins. Polyreactivity ELISA was performed as previously described (Prigent et al., 2016). Briefly, high-binding 96-well ELISA plates (Costar, Corning, Corning, NY) were coated overnight with 500 ng/well of purified double stranded (ds)-DNA, KLH, LPS (Sigma), 250 ng/well of insulin (Sigma), and 125 ng/well of HIV-1 proteins in PBS. After blocking and washing steps, purified IgG antibodies were tested in at 4 μg/ml and 3 consecutive 1:4 dilutions in PBS. Control antibodies, mGO53 (negative), and ED38 (high positive) were included in each experiment. After washings, the plates were revealed by incubation for 1 h with goat HRP-conjugated anti-human IgG or anti-human IgG/IgM/IgA antibodies (Immunology Jackson ImmunoReseach, 0.8 μg/ml final), and by adding 100 μl of HRP chromogenic substrate (ABTS solution, Euromedex) after washing steps. After 1 h incubation, optical densities were measured at 405nm (OD_{405nm}), and background values given by incubation of PBS alone in coated wells were subtracted. Experiments were performed using HydroSpeed microplate washer and Sunrise microplate absorbance reader (Tecan Männedorf,

Switzerland). For competition ELISAs, YU-2 gp140- and MN gp41-coated plates were blocked, washed, incubated for 2 h with biotinylated antibodies (at a concentration 0.33 nM) in 1:2 serially diluted solutions of antibody competitors in PBS (IgG concentration range from 1 to 133 nM), and developed as described above using HRP-conjugated streptavidin (BD Biosciences) (at 0.8 μg/ml in blocking buffer). High-binding 96-well ELISA plates (Costar, Corning) were coated overnight with purified recombinant MAPK14 (250 ng/well; Tebu-bio, Le Perray-en-Yvelines, France) and *E. coli* RNApol α (500 ng/well), and binding of HIV-1 antibodies was tested in the experimental conditions of our previously described peptide-ELISA method (Mouquet et al., 2006). Binding of anti-gp140 antibodies to gp41 peptides (NIH Reagent Program) was tested using the same procedure as in (Mouquet et al., 2006). To determine the ionic strength dependence of the antibody-antigen interactions, MAPK14 ELISAs were performed as described above but with antibodies diluted in 10 mM HEPES pH 7.3 containing different concentrations of NaCl – 0.125, 0.25, 0.5, and 1 M. All antibodies were tested in duplicate (excepted for the polyreactivity testing of non HIV-1 antibodies) in at least two independent experiments, which included mGO53 negative and appropriate positive controls.

HIV-1 virus production and *in vitro* neutralization assay

Pseudoviruses (Bal.26, 6535.3, YU-2, SC422661.8 and PVO.4; Env plasmids obtained from the NIH AIDS reagent program) were prepared by cotransfection of 293T cells with pSG3ΔEnv vector using FUGENE-6 transfection reagent (Promega, Madison, WI) as previously described (Li et al., 2005; Sarzotti-Kelsoe et al., 2014). Pseudoviruses-containing culture supernatants were harvested 2 days post-transfection and 50% tissue culture infectious dose (TCID50) of each preparation was determined using TZM-bl cells as previously described (Li et al., 2005; Sarzotti-Kelsoe et al., 2014). Neutralization of cell-free HIV-1 was measured using TZM-bl cells as previously described (Li et al., 2005; Sarzotti-Kelsoe et al., 2014). The 50% inhibitory concentration (IC_{50}) values were calculated using GraphPad Prism software (v6.0a, GraphPad Prism Inc., USA) by fitting duplicate values using the 5-parameters sigmoidal dose-response model. Neutralization experiments were performed twice and included mGO53 negative control.

In vitro viral transcytosis assay

Transcytosis assays were performed using epithelial monolayer-forming human endometrial carcinoma type A HEC-1A cells (ATCC® HTB-112) cultivated on 0.4 μm polyethylene terephthalate transwell membranes (Millicell®, Millipore) as recently described (Lorin et al., 2017). Briefly, the confluence, tightness and integrity of HEC-1A monolayers were controlled by measuring the transepithelial electrical resistance, the paracellular permeability to 40 kDa FITC-labeled DEAE-dextran (Molecular Probes) and by assaying the expression of tight junction proteins by confocal microscopy as previously described (Lorin et al., 2017). HIV-1 viruses (10 ng of p24 HIV-1 NLAD8) were incubated v/v for 1 h at 37°C with purified antibodies (66.67 nM final concentration), and mixtures were added onto HEC-1A monolayers at day 6 of culture. As controls, HIV-1 alone was added into inserts with cells (No Ab) and without cells (CTL), which takes into account the proportion of virions not passing through the transwell filter. After 24 h, basal media were collected and their p24 content measured by ELISA (HIV-1 p24 Antigen Capture Assay, Advanced Bioscience Laboratories Inc., Rockville, MD). The percentage of transcytosis was determined using the following formula: (concentration p24 sample / mean concentration p24 CTL)*100. The infectivity of virions transcytosed in the presence or not of antibodies (0.05 ng p24) was measured using a previously described TZM-bl cells assay (Lorin et al., 2017). Two independent experiments were performed in quadruplicate, and included negative (mGO53) and positive (10-1074) controls.

Flow cytometry binding analysis to infected cells

Laboratory-adapted (NL4.3, AD8 and YU-2) and T/F (WITO, CH058, CH077, CH0106, REJO and RHPA) (Ochsenbauer et al., 2012) viruses were produced from infectious molecular clones (NIH AIDS Reagent Program) as previously described (Casartelli et al., 2010). CEM-NKR-CCR5 cells (NIH AIDS Reagent Program) were infected with inocula of selected viruses, and adjusted to achieve 10%–30% of Gag^+ cells at 48 h post infection (Bruel et al., 2016; Bruel et al., 2017). Infected cells were incubated with IgG antibodies (at 15 μg/ml) in staining buffer (PBS, 0.5% BSA, 2mM EDTA) for 30 min at 37°C, washed and incubated 30 min at 4°C with AF647-conjugated anti-human IgG antibodies (1:400 dilution; Life technologies). Cells were then fixed with 4% paraformaldehyde and stained for intra-cellular Gag as previously described (Bruel et al., 2016; Bruel et al., 2017). Data were acquired using an Attune Nxt instrument (Life Technologies) and analyzed using FlowJo software (v10.3; FlowJo LLC).

Viral capture assay

High-binding 96-well ELISA plates (Costar, Corning) were coated overnight with goat anti-human IgG antibodies (250 ng/well, Jackson Immunoreasearch) in PBS. After washings in PBS, plates were blocked 2 h with 5% non-fat dry milk in PBS, and then incubated 2 h with 500 ng/well of IgGs in PBS. After three washes, 10 ng p24 HIV-1 virions in 10%FBS-DMEM medium (GIBCO, Life technologies) were added *per* well. Plates were incubated 4 h at 37°C, extensively washed with PBS and captured HIV-1 virions were lysed with 100 μl of lysis buffer (100μl/well, Advanced Bioscience Laboratories Inc.). The amount of captured virions was determined as p24 content using the HIV-1 p24 Antigen Capture Assay (Advanced Bioscience Laboratories Inc.) according to the manufacturer's instructions. Samples were analyzed in quadruplicate.

ADCC assay

The ADCC assay was performed as previously described (Bruel et al., 2016; Bruel et al., 2017). Briefly, 2 × 10^4 HIV-1-infected CEM-NKR cells stained with Far-Red cell tracker (Life Technologies) were incubated with antibodies (at 15 μg/ml) for 5 min at room temperature. Primary NK cells (2 × 10^5) were added to each well, with a ratio of 1 CEM-NKR cell to 10 NK cells. Plates were then spun for 1 min at 300 g and incubated at 37°C for 4 h. After fixation with 4% PFA for 10 min, cells were stained for intracellular Gag as previously described (Bruel et al., 2016; Bruel et al., 2017). Data were acquired on an Attune Nxt instrument (Life Technologies) and analyzed using FlowJo software (v10.3; FlowJo LLC). The frequencies of Gag^+ cells among $Far\text{-}Red^+$ cells were determined. ADCC was calculated by using the following formula: 100 × (% of Gag^+ target cells *plus* NK cells without antibody - % of Gag^+ target cells *plus* effector cells with antibody) / (% of Gag^+ target cells *plus* NK cells without antibody). Negative values were set to zero. mGO53 negative control was included in each experiment.

SPR binding assay

To measure the apparent affinity of IgG antibodies to YU-2 and ZM-96 trimers, CM5 chips (Biacore, Inc.) were immobilized by using Amine Coupling Kit (Biacore, GE Healthcare) to reach immobilization levels of 600 and 800 RUs, respectively. MAPK14 was immobilized in the same conditions to reach 50 and 250 RUs immobilization levels. IgGs at a concentration of 1 μM (for 18-295, HD1a361 and HD2a57), 0.5 μM (for ED38), 125 nM (for 64-i109) or 62.5 nM (for 6-104 and 6-195) for HIV-1 trimers and 250 nM of each antibody for MAPK14, and 6-8 successive 1:2 dilution in HBS-EP+ running buffer (Biacore, GE Healthcare) were injected through flow cells at flow rates of 30 μl/min with 3 min association and 4 min dissociation. The sensor surface was regenerated between each experiment with a 30-60 s injection of 4 M $MgCl_2$ and 1M NaCl-0.05 M NaOH for HIV-1 Env- and MAPK14-immobilized chips, respectively. All experiments were performed with a Biacore 2000 (Biacore, GE Healthcare) at 25°C. Evaluation of kinetic data was performed using the BIAevaluation software (v4.1.1, Biacore, GE Healthcare) by applying 1:1 binding Langmuir model or alternatively, using equilibrium analyses when the 1:1 fitting was not possible.

HEp-2 IFA

Recombinant mucosal IgG antibodies and control antibodies (mGO53 and ED38) at 150 μg/ml were analyzed by indirect immunofluorescence assay (IFA) on HEp-2 cells sections (ANA HEp-2 AeskuSlides®, Aesku.Diagnostics, Wendelsheim, Germany) using the kit's controls and FITC-conjugated anti-human IgG antibodies as the tracer according to the manufacturer' instructions. Sections were examined using the fluorescence microscope Axio Imager 2 (Zeiss, Jena, Germany) with ApoTome.2 system, and pictures were taken at magnification x 40 with 7000 ms-acquisition using ZEN imaging software (Zen 2.0 blue version, Zeiss) at the Imagopole platform (Institut Pasteur).

Protein microarray binding analyses

All experiments were performed at 4°C using ProtoArray Human Protein Microarrays (Thermo Fisher Scientific). Microarrays equilibrated at 4°C for 15 min were then blocked for 1h in blocking solution (50 mM HEPES pH 7.5, 200 mM NaCl, 0.08% Triton X-100, 20 mM reduced glutathione, 1 mM DTT, 25% glycerol, 1 X synthetic block; Thermo Fisher) under gentle shaking (50 rpm). After 5 washes in 0.1% Tween 20-PBS (5 min each) and once in synthetic block, protein arrays were incubated for 1h30 with IgG antibodies at 2.5 μg/ml in 0.1% Tween 20-PBS (under 50 rpm shaking). After washings (as above), arrays were incubated for 1h30 with Alexa Fluor 647-conjugated goat-anti human IgG (at 1 μg/ml in PBS; Thermo Fisher Scientific). After washings (as above), arrays were soaked in deionized water and dried by centrifugation at 200 x g for 1 min. Fluorescence on microarrays was detected using GenePix 4000B microarray scanner (Molecular Devices) and GenePix Pro 6.0 software (Molecular Devices) with 100% laser power, PMT 400V and a spot resolution of 10 μm. Fluorescence intensities were quantified using Spotxel® software (SICASYS Software GmbH, Germany). Mean fluorescence intensity (MFI) signals for each antibody (from duplicate protein spots) was plotted against the reference antibody mGO53 (isotype, non-HIV-1, non polyreactive control) using GraphPad Prism software (v6.0a, GraphPad Prism Inc.). For each antibody, Z-scores were calculated using ProtoArray® Prospector software (v5.2.3, Thermo Fisher Scientific), and were plotted against mGO53 antibody control as reference. Deviation (σ) to the diagonal line y = x, and polyreactivity index (PI) values were calculated as previously described (Liu et al., 2015). The PI corresponds to the Gaussian mean of protein MFI distances from the y = x line plotted in GraphPad Prism software (v6.0a, GraphPad Prism Inc.). Antibodies were defined as polyreactive when PI > 0.21 (Liu et al., 2015). The crossreactivity testing for the 4 mucosal HIV-1 antibodies were performed in 2 independent experiments. Sequence alignments based on the structural superposition between $gp41^{HR2}$ cluster II peptite (from PDB ID: 1ENV) and MAPK14 (PDB ID: 5ETI) were performed using the MatchMaker command of the UCSF Chimera software (v1.9; [Meng et al., 2006]).

QUANTIFICATION AND STATISTICAL ANALYSIS

The numbers of V_H, Vκ and Vλ mutations were compared across groups of antibodies using unpaired Student's t test with Welch's correction. Percentages of transcytosis and levels of infectivity were compared for each antibody to mGO53 negative control group using Mann-Whitney test. Bivariate correlations were assayed using two-tailed Pearson correlation test. Statistical analyses were performed using GraphPad Prism software (v6.0a, GraphPad Prism Inc.).

Cell Reports, Volume *27*

Supplemental Information

HIV-1 Envelope Recognition by Polyreactive and Cross-Reactive Intestinal B Cells

Cyril Planchais, Ayrin Kök, Alexia Kanyavuz, Valérie Lorin, Timothée Bruel, Florence Guivel-Benhassine, Tim Rollenske, Julie Prigent, Thierry Hieu, Thierry Prazuck, Laurent Lefrou, Hedda Wardemann, Olivier Schwartz, Jordan D. Dimitrov, Laurent Hocqueloux, and Hugo Mouquet

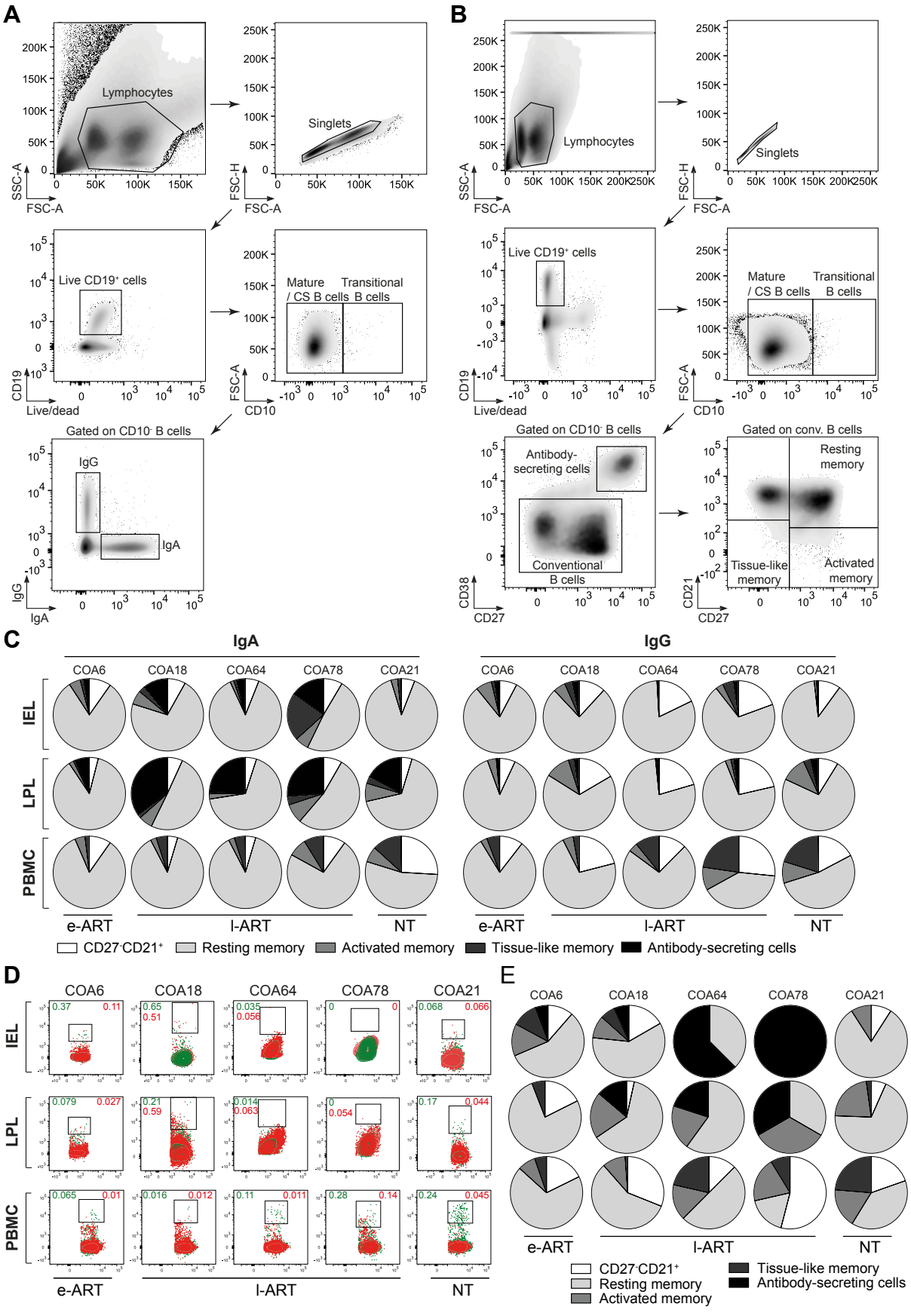

Figure S1. Immunophenotyping of mucosal B-cell subsets from HIV-1-infected individuals (n=5). Related to Figure 1. (**A**) Cytograms show the gating strategy used in flow cytometry analyses to calculate the frequency of the mucosal IgA$^+$ and IgG$^+$ B cells in patients' rectosigmoid biopsies as shown in Figure 1C. (**B**) Cytograms show the gating strategy used in flow cytometry analyses for the immunophenotyping and frequency calculation of the mucosal B-cell subsets in patients' rectosigmoid biopsies as shown in Figure 1D. (**C**) Pie charts comparing the distribution of B-cell subsets in the IEL, LPL and PBMC compartments as determined by flow cytometry for the 5 HIV-1-infected individuals. (**D**) Cytograms show for each donor (n=5), the proportion of single gp140-binding cells among IgG$^+$ and IgA$^+$ B cells. (Bottom) Dot plots comparing the % of IgA$^+$ and IgG$^+$ gp140-reactive B cells. (**E**) Pie charts comparing the distribution of single gp140-binding B cells in the IEL, LPL and PBMC compartments as determined by flow cytometry for the 5 HIV-1-infected individuals.

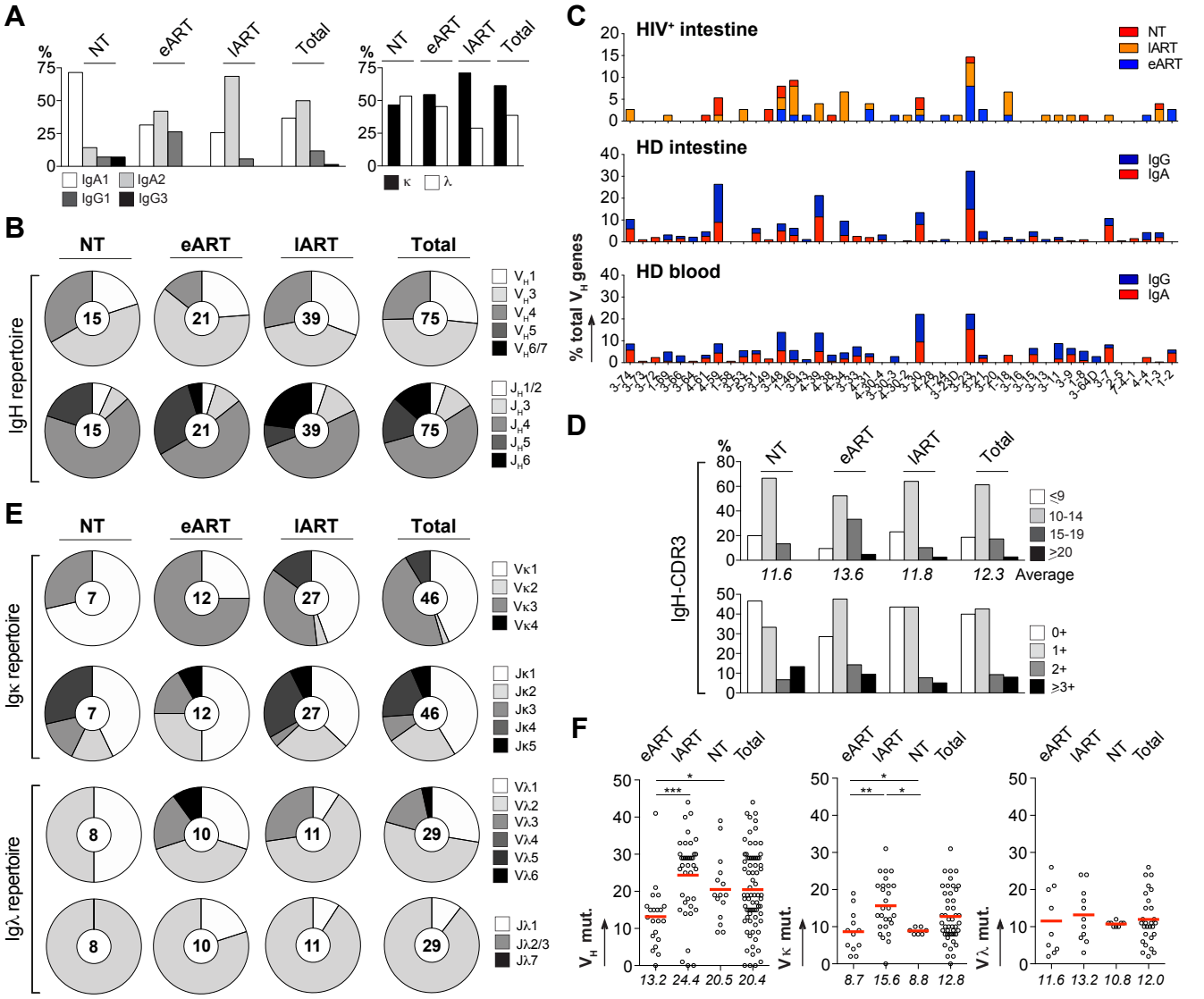

Figure S2. Immunoglobulin gene repertoire of gp140-captured intestinal B cells from HIV-1-infected individuals (n=5). Related to Figure 1. (**A**) Bar graphs show the distribution of IgG/IgA subtypes (Left) and κ- vs λ-Ig chain usage (Right) in gp140-captured mucosal B cells. (**B**) IgH and IgL gene usages. Pie charts show the distribution of V_H / J_H gene usage in gp140-captured mucosal B cells. The number of antibody sequences analyzed is indicated in the center of each pie chart. (**C**) Bar graph comparing the distribution of single immunoglobulin V_H genes expressed by intestinal B cells of HIV-1-infected donors (combining NT, eART and lART donors), total intestinal IgG^+/IgA^+ plasmablasts (Benckert et al., 2011) and blood IgG^+/IgA^+ memory B cells (Prigent et al., 2016) from healthy individuals. (**D**) Bar graphs show the distribution of CDR_H3 lengths and positive charge numbers in gp140-captured mucosal B cells. The average of CDR_H3 lengths is indicated above each histogram. (**E**) Pie charts show the distribution of $V_κ$ / $J_κ$ and $V_λ$ / $J_λ$ gene usage in gp140-captured mucosal B cells. The number of antibody sequences analyzed is indicated in the center of each pie chart. (**F**) Dot plots show the number of mutations in V_H, Vκ and Vλ genes gp140-captured mucosal B cells. The average number of mutations (mut.) is indicated below each dot plot. Numbers of mutations were compared across groups of antibodies using unpaired student t-test with Welch's correction. *, p<0.05; **, p<0.01; ***, p<0.001.

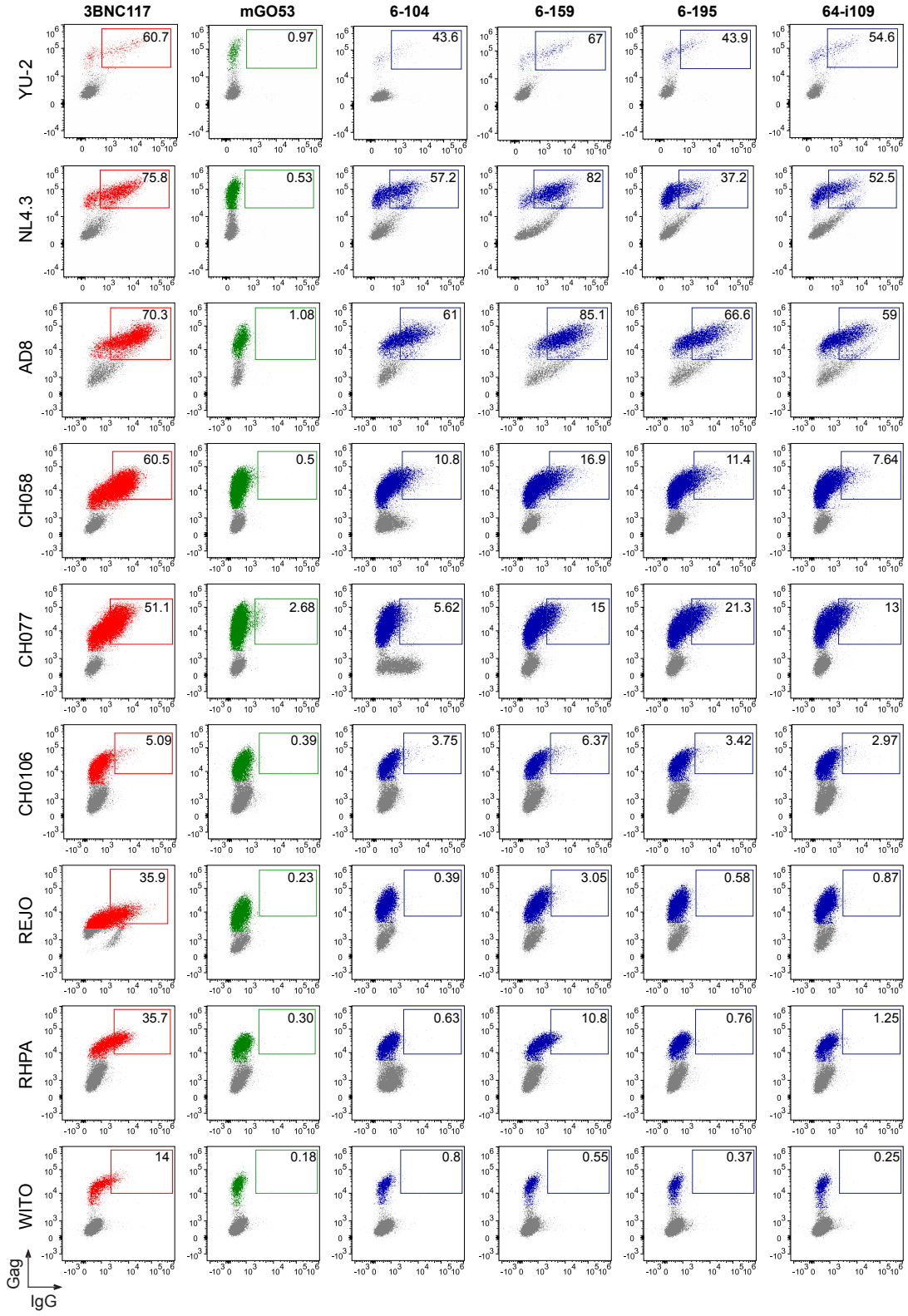

Figure S3. Binding of mucosal gp160-specific antibodies to HIV-1-infected cells. Related to Figure 2. Representative cytograms show the binding of mucosal anti-gp140 and control IgG antibodies to Gag^+ target cells infected with the selected viruses. 3BNC117 (Scheid et al., 2011) and mGO53 (Wardemann et al., 2003) are positive and negative control, respectively. The % of Gag^+ cells bound by antibody is indicated in the right-end upper corner of the gate.

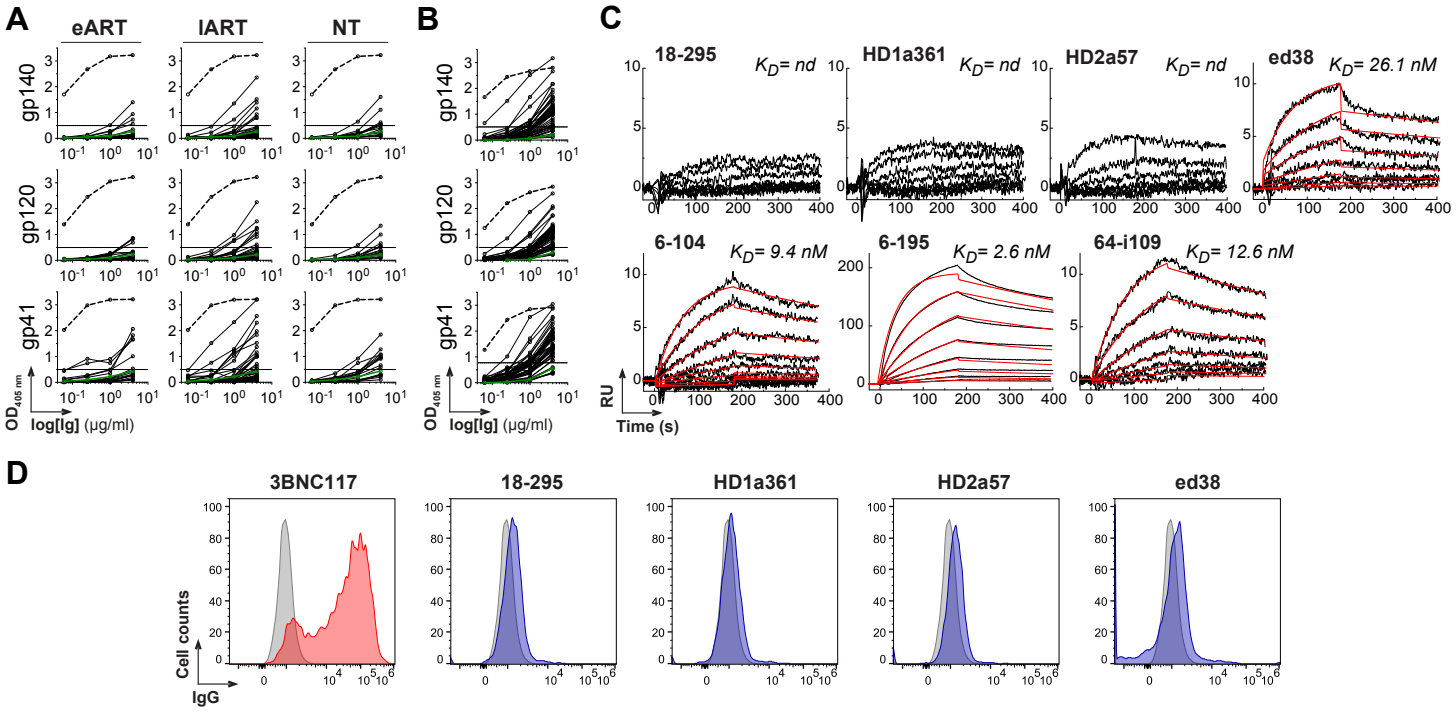

Figure S4. Polyreactive binding to HIV-1 envelope proteins. Related to Figure 3. (**A**) ELISA graphs show the reactivity of intestinal IgG mAbs from mucosal antibodies isolated from HIV-1-infected individuals (n=72) against clade B trimeric gp140, gp120 and gp41 proteins in the experimental conditions to measure polyreactivity (see Experimental Procedures). mGO53 (Wardemann et al., 2003) (green lines) and ED38 (Meffre et al., 2004) (dotted lines) are negative and positive control antibody, respectively. Horizontal lines show cut-off $OD_{405\ nm}$ for positive reactivity. Mean values from two independent experiments are shown. (**B**) Same as for (A) but for polyreactive intestinal IgG mAbs from healthy individuals (n=41) (Benckert et al., 2011). (**C**) SPR sensorgrams comparing the binding of selected antibodies to trimeric ZM96 gp140 glycoproteins. The y axis shows the response units (RU) obtained at a given time (s, seconds) indicated on the x axis. (**D**) Flow cytometry histograms show the binding of selected IgGs to YU-2-infected cells (colored) compared to non-infected target cells (grey). 3BNC117 (Scheid et al., 2011) is the positive control.

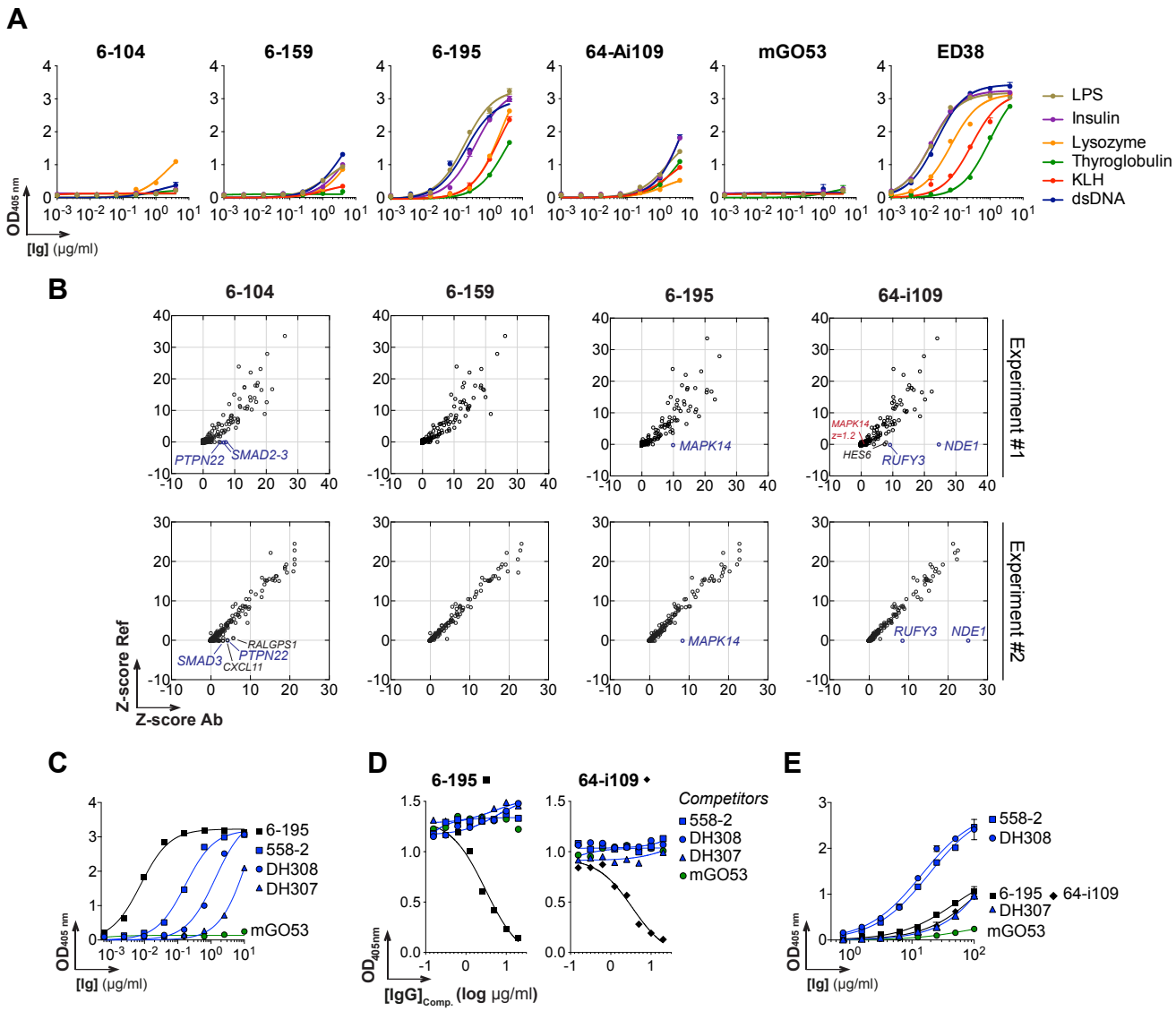

Figure S5. Poly- and cross-reactivity of mucosal HIV-1 antibodies. Related to Figure 4. (**A**) Representative ELISA graphs show the reactivity of mucosal HIV-1 antibodies against dsDNA, ssDNA, insulin, keyhole limpet hemocyanin (KLH), thyroglobulin and lysozyme. mGO53 (Wardemann et al., 2003) and ED38 (Meffre et al., 2004) are negative and positive control antibody, respectively. Mean of duplicate values are shown. (**B**) Protein microarray plots show the reactivity profile of mucosal anti-gp140 antibodies against human proteins obtained in two independent experiments. For each protein spot, Z-scores given by the reference (Ref: mGO53) and test antibody are depicted on the y and x axis, respectively. Blue dots correspond to the immunoreactive proteins identified in both experiments. RALGPS1, Ral GEF with PH domain and SH3 binding motif 1. (**C**) ELISA graphs show the reactivity of previoulsy cloned mucosal anti-gp41 cluster I antibodies (Liao et al., 2011; Trama et al., 2014) to MN gp41. mGO53 and 6-195 are negative and positive control antibody, respectively. Mean of duplicate values are shown. (**D**) ELISA graphs show the binding of biotinylated 6-195 and 64-i109 antibodies to gp41 in the presence of mucosal anti-gp41 cluster I antibodies (Liao et al., 2011; Trama et al., 2014). Mean of duplicate values are shown. (**E**) Representative ELISA graphs show the reactivity of the selected antibodies to E. coli RNA polymerase subunit a. mGO53 is the negative control. Error bars indicate the SEM of duplicate values.

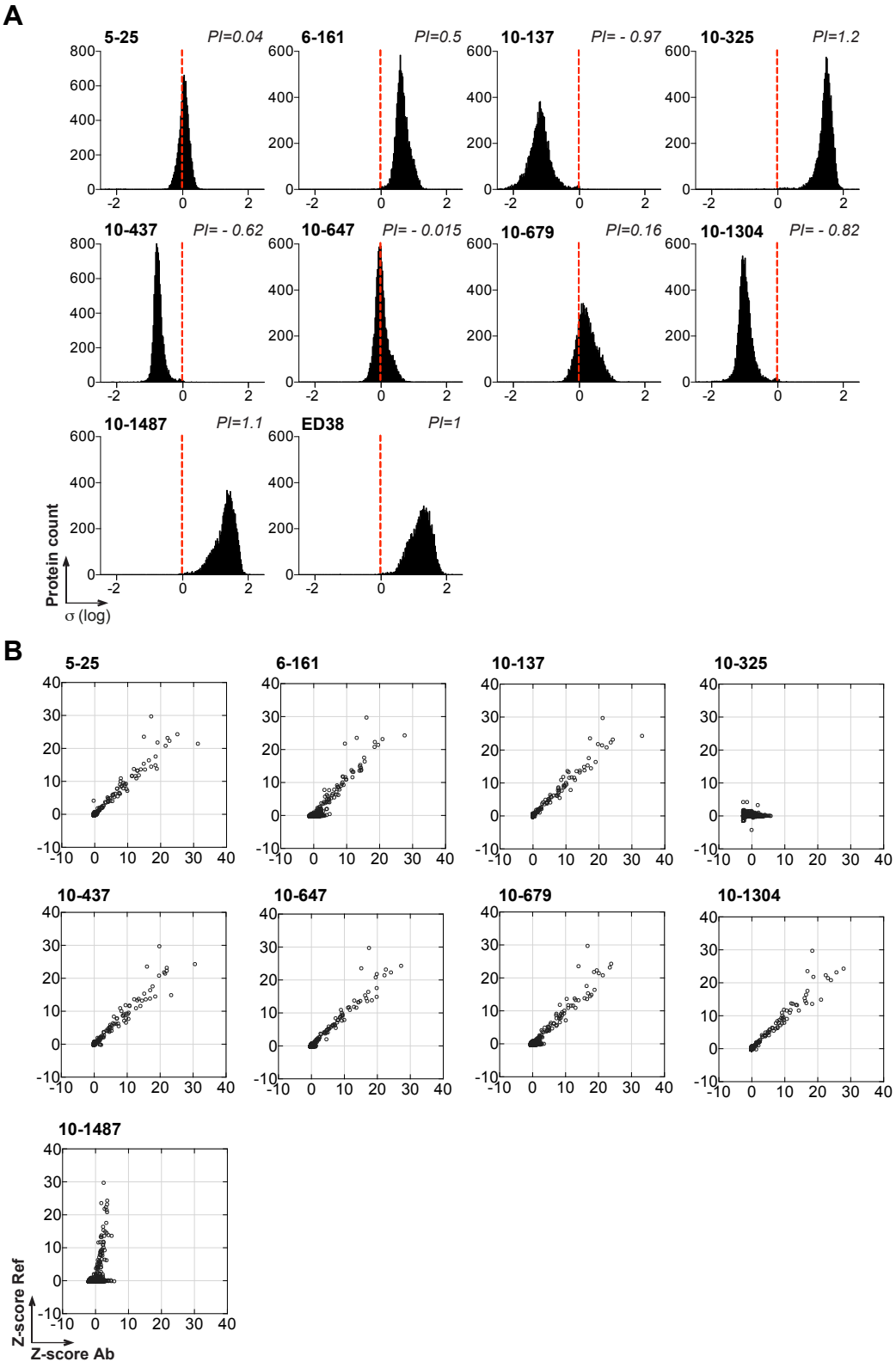

Figure S6. Poly- and cross-reactivity of blood HIV-1 gp41 antibodies. Related to Figure 5. (**A**) Frequency histograms show the $\log_{10}$ protein displacement (σ) of the MFI signals for the selected antibodies compared to non-HIV-1 control antibody mGO53 (Wardemann et al., 2003). The polyreactivity index (PI) corresponds to the Gaussian mean of all array protein displacements. (**B**) Protein microarray plots show the reactivity profile of mucosal anti-gp140 antibodies against human proteins. For each protein spot, Z-scores given by the reference (Ref: mGO53) and test antibody are depicted on the y and x axis, respectively.

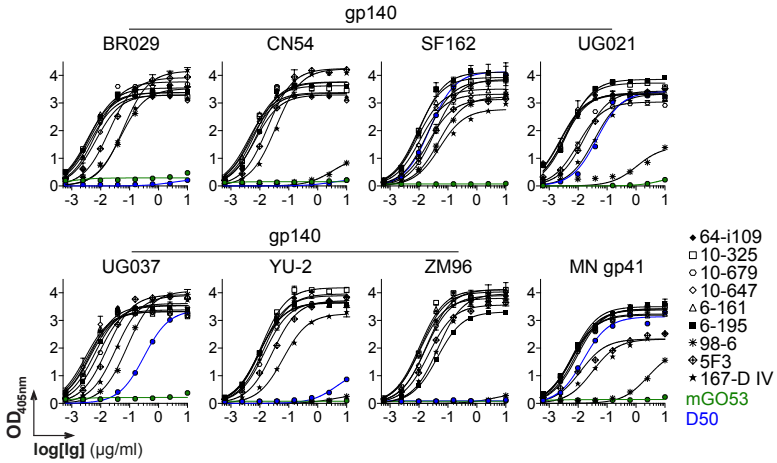

Figure S7. Reactivity of anti-gp41^{HR2} antibodies to various HIV-1 Env proteins. Related to Figure 6. ELISA graphs show the reactivity of human anti-gp41^{HR2} (Gorny et al., 1989; Xu et al., 1991; Buchacher et al., 1994; Scheid et al., 2009; Mouquet et al., 2011), and murine D50 (Earl et al., 1997) antibodies to the selected trimeric gp140 and gp41 proteins. mGO53 (Wardemann et al., 2003) is the negative control. Error bars indicate the SEM of duplicate values.